สมดุลการดูดซับสารเบนซีน โทลูอีน และไซลีน บนเส้นใยคาร์บอนนาโนจากพอลิอะคริโลไนไทร์ล
ที่มีแมงกานีสฝังตัวอยู่ โดยเตรียมจากการปั่นเส้นใยด้วยไฟฟ้าสถิตย์

นางสาวญาณิศา แก้วมณี

วิทยานิพนธ์นี้เป็นส่วนหนึ่งของการศึกษาตามหลักสูตรปริญญาวิศวกรรมศาสตรมหาบัณฑิต
สาขาวิชาวิศวกรรมเคมี ภาควิชาวิศวกรรมเคมี
คณะวิศวกรรมศาสตร์ จุฬาลงกรณ์มหาวิทยาลัย
ปีการศึกษา 2556

ADSORPTION EQUILIBRIA OF BENZENE, TOLUENE, AND XYLENE ON MANGANESE-EMBEDDED PAN ACTIVATED CARBON NANOFIBERS FABLICATED BY ELECTROSPINNING

Miss Yanisa Kaewmanee

A Thesis Submitted in Partial Fulfillment of the Requirements
for the Degree of Master of Engineering Program in Chemical Engineering
Department of Chemical Engineering
Faculty of Engineering
Chulalongkorn University
Academic Year 2013

Thesis Title	ADSORPTION EQUILIBRIA OF BENZENE, TOLUENE, AND XYLENE ON MANGANESE-EMBEDDED PAN ACTIVATED CARBON NANOFIBERS FABLICATED BY ELECTROSPINNING
By	Miss Yanisa Kaewmanee
Field of Study	Chemical Engineering
Thesis Advisor	Assistant Professor Varong Pavarajarn, Ph.D.

Accepted by the Faculty of Engineering, Chulalongkorn University in Partial Fulfillment of the Requirements for the Master's Degree

.....Dean of the Faculty of Engineering

(Professor Bandhit Eua-arporn, Ph.D.)

THESIS COMMITTEE

.....Chairman

(Professor Suthichai Assabumrungrat, Ph.D.)

.....Thesis Advisor

(Assistant Professor Varong Pavarajarn, Ph.D.)

.....Examiner

(Associate Professor Artiwan Shotipruk, Ph.D.)

.....External Examiner

(Busarakam Charnhattakorn, Ph.D.)

ญาณิศา แก้วมณี : สมดุลการดูดซับสารเบนซีน โทลูอีน และไซลีน บนเส้นใยคาร์บอนนาโนจากพอลิอะคริโลไนไทร์ล ที่มีแมงกานีสฝังตัวอยู่ โดยเตรียมจากการปั่นเส้นใยด้วยไฟฟ้าสถิตย์. (ADSORPTION EQUILIBRIA OF BENZENE, TOLUENE, AND XYLENE ON MANGANESE-EMBEDDED PAN ACTIVATED CARBON NANOFIBERS FABLICATED BY ELECTROSPINNING) อ.ที่ปรึกษาวิทยานิพนธ์หลัก: ผศ. ดร. วรงค์ ปวราจารย์, 83 หน้า.

ในงานวิจัยนี้ เป็นการเตรียมเส้นใยคาร์บอนนาโนจากพอลิอะคริโลไนไทร์ลที่มีแมงกานีสฝังตัวอยู่ โดยเตรียมจากการปั่นเส้นใยด้วยไฟฟ้าสถิตย์ เส้นผ่านศูนย์กลางของเส้นใยพอลิอะคริโลไนไตร์ลอยู่ในช่วง 200 ถึง 500 นาโนเมตร โดยนำเส้นใยที่เตรียมได้มาผ่านกระบวนการปรับสภาพที่อุณหภูมิ 280 องศาเซลเซียสในบรรยากาศของอากาศ นำมาเผาให้กลายเป็นคาร์บอนที่ช่วงอุณหภูมิ 800 ถึง 1,000 องศาเซลเซียสในบรรยากาศของไนโตรเจน และทำการกระตุ้นด้วยไอน้ำที่ 800 องศาเซลเซียส จะได้ตัวอย่างที่เป็นเส้นใยคาร์บอนนาโน มีผลผลิตร้อยละของเส้นใยคาร์บอนนาโนที่เตรียมจาก 8 เปอร์เซ็นต์ของสารละลายพอลิอะคริโลไนไทร์ลที่ผ่านการเผาที่อุณหภูมิ 800, 900 และ 1,000 องศาเซลเซียส เป็น 2, 10 และ 10 เปอร์เซ็นต์ ตามลำดับ ในขณะที่ผลผลิตร้อยละของ 10 เปอร์เซ็นต์ของสารละลายพอลิอะคริโลไนไทร์ลเป็น 20, 16 และ 15 เปอร์เซ็นต์ ตามลำดับ

เมื่อนำเส้นใยคาร์บอนนาโนที่เตรียมได้มาทำการดูดซับไอของโทลูอีน พบว่าเส้นใยคาร์บอนนาโนที่เผาที่ 1,000 องศาเซลเซียส สามารถดูดซับโทลูอีนได้มากที่สุด คือ 26.83 กรัมของโทลูอีนต่อ 100 กรัมของตัวดูดซับ เนื่องจากมีปริมาตรรูพรุนทั้งหมดสูงกว่าตัวอย่างอื่นๆ มีขนาดรูพรุนเฉลี่ยที่ใหญ่กว่า แต่เมื่อเปรียบเทียบกับงานวิจัยอื่นๆ พบว่ายังมีพื้นที่ผิวจำเพาะที่น้อยกว่า และมีอัตราส่วนของออกซิเจนต่อคาร์บอนในโครงสร้างสูง ซึ่งในการเติมแมงกานีสลงไปในเส้นใยคาร์บอนไม่ได้ช่วยให้การดูดซับโทลูอีนดีขึ้น เนื่องจากสภาวะในการกระตุ้นให้เป็นถ่านกัมมันต์ใช้ไอน้ำที่ความหนาแน่นและความดันต่ำเกินไป อีกทั้งปริมาณของแมงกานีสที่เหลืออยู่ในตัวอย่างเกิดการรวมตัวเป็นกระจุกขนาดใหญ่ที่พื้นผิวของตัวอย่าง ซึ่งอาจขัดขวางการปรับปรุงพื้นผิวของตัวอย่าง

ภาควิชา วิศวกรรมเคมี ลายมือชื่อนิสิต .....

สาขาวิชา วิศวกรรมเคมี ลายมือชื่อ อ.ที่ปรึกษาวิทยานิพนธ์หลัก .....

ปีการศึกษา 2556

5371476421 : MAJOR CHEMICAL ENGINEERING
KEYWORDS: ACTIVATED CARBON NANOFIBERS / ADSORPTION / TOLUENE

YANISA KAEWMANEE: ADSORPTION EQUILIBRIA OF BENZENE, TOLUENE, AND XYLENE ON MANGANESE-EMBEDDED PAN ACTIVATED CARBON NANOFIBERS FABLICATED BY ELECTROSPINNING. ADVISOR: ASST. PROF. VARONG PAVARAJARN, Ph.D., 83 pp.

In this research, manganese-embedded activated carbon nanofibers (ACNFs) were prepared from electrospun polyacrylonitrile (PAN) nanofibers. The average diameter of the PAN fibers was in the range of 200 to 500 nm. After stabilization at 280 ℃ in air, carbonization at temperature in the range of 800 to 1,000 ℃ in nitrogen, and activation by steam at 800 ℃, the ACNFs were obtained. The activation yield of the nanofibers formed from 10% PAN solution and carbonized at 800, 900 and 1,000 ℃ were 20%, 16% and 15%, respectively. Meanwhile the activation yield of the fibers electrospun from 8% PAN solution and carbonized at 800, 900 and 1,000 ℃ were 2%, 10% and 10%, respectively. The functional groups of ACNFs were different from that of polymer fibers. The results showed that the ACNF carbonized at 1,000 ℃ showed the highest toluene adsorption capacity of 26.83 g toluene/100 g adsorbent due to the highest total pore volume and large mean pore diameter. However when compared to other research, the specific surface area was still lower while having high O/C ratio. Moreover, manganese did not enhance toluene adsorption capacity because steam density and pressure used in the activation was low and remaining manganese in ACNFs become agglomerated on surface and interrupt activation process.

Department: Chemical Engineering Student's Signature .....

Field of Study: Chemical Engineering Advisor's Signature .....

Academic Year: 2013

ACKNOWLEDGEMENTS

Foremost, the author would like to express her sincere gratitude and appreciation to her advisor Assistant Professor Dr. Varong Pavarajarn, for his introducing this interesting subject with the continuous support, patience, motivation, enthusiasm, and immense knowledge throughout this thesis.

The author acknowledges the financial support provided by Chulalongkorn University.

The author is similarly grateful to Professor Dr. Suthichai Assabumrungrat as the chairman, Associate Professor Dr. Artiwan Shotipruk as the thesis committee, and Dr. Busarakam Charnhattakorn as the external thesis examiner, for their encouragement, insightful comments, and useful questions.

The author would like to thank the member of the Center of Excellence on Particle Technology, Faculty of Engineering, Chulalongkorn University for their assistance and suggestion.

Last but not the least; the author would like to thank her family for supporting her spiritually throughout her life.

CONTENTS

Page

Page

Page

LIST OF TABLES

LIST OF FIGURES

LIST OF FIGURES (Cont.)

CHAPTER 1
INTRODUCTION

1.1 Background

Nowadays, in Thailand faces many environmental issues especially air pollution. One of major source is from industrial discharges with no appropriate air pollution treatment system, particularly volatile organic compounds (VOCs). The conventional method for VOCs treatment commonly is adsorption by using activated carbon but have some disadvantage such as flammable and low capacity of VOCs per weight of activated carbon. In this research aim to develop activated carbon nanofibers to have more VOCs adsorption capacity.

Benzene, toluene and xylene (BTX) are VOCs found in broad range of industries. The American Conference of Governmental Industrial Hygiene (ACGIH) has classified these compounds as type 1:A1, which is identified as carcinogen in humans [1]. In environment field, BTX react with oxides of nitrogen in the atmosphere under sunlight become ozone can cause eye irritation and irritate to the respiratory system, the ability decline in lung function, especially in children soon tired, elderly and people with chronic lung disease. [2]

Adsorption is an effective technique that has been used to remove the VOCs [3]. In the adsorption, the contaminants diffuse and adhere to the outer surface of the adsorbent. Therefore, a good adsorbent must have large surface and high porosity.

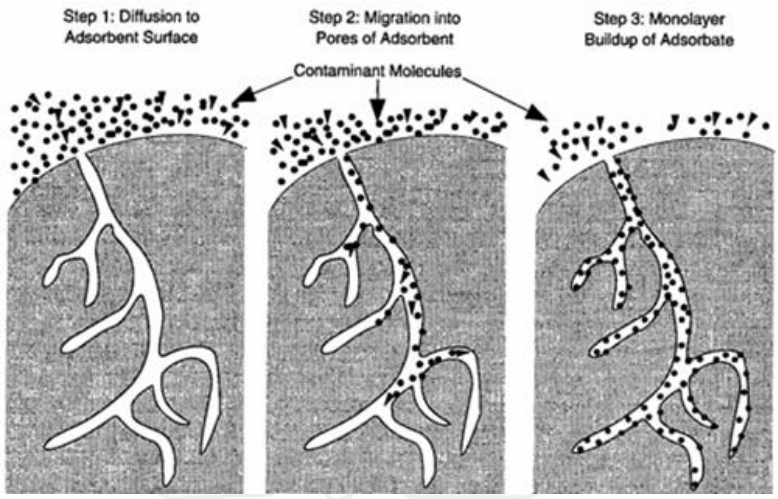

Fig. 1 Adsorption mechanism [3]

Ultrafine fiber is an exciting new class of materials used for several value added applications such as medical, filtration, barrier, wipes, personal care, composite, garments, insulation and energy storage. Special properties of nanofibers make them suitable for a wide range of applications from medical to consumer products and industrial to high-tech applications for aerospace, capacitors, transistors, drug delivery systems, battery separators, energy storage, fuel cells and information technology [4, 5]. Ultrafine fibers produced by electrospinning technology come from polymer solutions. The polymer used is the most important parameter that defines the properties of the final ultrafine fibrous fabric [6].

Carbon nanofibers have been used to as an adsorbent for the removal of VOCs including BTX. Factors affecting the adsorption of the organic compounds include surface area, pore structure as well as activation of the surface of the carbon [7].

Electrospinning is a technique to spin polymer fibers with diameter in nanometer scales by using electrical field to apply both polymer solution and a collector plate to force a polymer jet out of the needle tip during spinning, which employs high voltages to stretch a droplet of polymer solution into fine jets, which consequently solidify into nanofibers and deposit on the metal collector. The fibers made from the electrospinning process are nano-sized in diameter and normally non-woven fibers. Some parameters must be concerned such as applied voltage, polymer solution concentration, distance between needle tip and collector plate and also electrical conductivity of polymer solution [8].

Polyacrylonitrile (PAN), which is one of the most common polymers used in the manufacture of carbon fibers, has been discovered since 1960. Yield of the carbon fibers obtained via the pyrolysis of the as-spun PAN fibers can be as high as 55%. The carbon nanofibers derived from PAN have also been used as adsorbent organic compounds [9-11]. However, further improvements such as activation of the fibers and introduction of metal clusters onto the fibers have been developed and proposed by many researchers to prevent the mesopore to occur so that the fibers are specific to adsorb BTX.

1.2 Objective of research work

1.1.1 To develop the electrospinning technique for fabricate manganese-embedded polyacrylonitrile (PAN) nanofibers.

1.1.2 To investigate pore characteristic and toluene adsorption capacity of synthesized carbon nanofibers prepared from difference carbonization temperature as well as concentration of PAN in the electrospinning solution.

1.1.3 To investigate effect of embedded-Mn in PAN nanofibers to enhance pore characteristics.

1.3 Scopes of research work

1.1.4 PAN with average molecular weight is 150,000 g/mol available from SIGMA-ALDRICH used as polymer solution for carbon source.

1.1.5 Manganese (II) acetate tetrahydrate available from SIGMA-ALDRICH used as Mn precursor in PAN solution.

1.1.6 N, N-Dimethylformamide (DMF) available from QRëC™ used as solvent.

1.1.7 Toluene available from QRëC™ used as vapor adsorbate.

1.1.8 Ethylene glycol available from POCH used as solvent for toluene calibration curve.

1.1.9 Lenton model: LTF, tube furnace for stabilized, carbonized, and activated the samples.

1.1.10 The conditions of electrospinning process are as follows

Applying voltage	: 20 kV
Distance between needle tip to collector	: 18 cm
Temperature and Humidity	: 22 ℃ and < 35 %RH

1.4 Expected benefits from this work

The obtained benefits from this research are the understanding of the pore characteristic of synthesized activated carbon nanofibers (ACNFs) and commercial activated carbon and apply to adsorb maximize toluene vapor with optimal carbonization temperature and activated condition.

CHAPTER 2
THEORY AND LITERATURE REVIEW

2.1 Concepts and theories

In this research, toluene adsorbent, ACNFs were prepared from manganese-embedded PAN nanofiber by electrospinning process, heat stabilization, carbonization, and activation.

2.1.1 Electrospinning process

Nanofibers are polymer fibers that having diameters of less than one micron or less in the nanoscales. When the diameters of polymer fiber materials are down from micrometers (10^{-6} m) to nanometers (10^{-9} m), they appear to have several amazing characteristics such as very large surface area to volume ratio, flexibility in surface functionalities, and superior mechanical performance (e.g. stiffness and tensile strength) compared with other materials. These outstanding properties make the polymer nanofibers to be optimal candidates for many important applications such as medical and filtration applications. An electrospinning technique has been used to produce polymer nanofibers.

Electrospinning is the process that using electrostatic force to generate the fine filament. The electrospinning set up is shown in Fig. 2 which consists of an adjustable DC power supply for applying the voltage, a glass syringe is connected to a stainless steel needle using a teflon tube having an inner diameter of 1.1 mm, and collector wrapped with aluminum foil [12].

In the electrospinning process a high voltage is used to create an electrically charged jet of polymer solution or melt, which dries or solidifies to leave polymer fibers. One electrode is placed into the spinning solution/melt and the other attached to a collector. Electric field is subjected to the end of a capillary tube that contains the polymer fluid held by its surface tension. This induces a charge on the surface of the liquid. Mutual charge repulsion causes a force directly opposite to the surface tension. As the intensity of the electric field is increased, the hemispherical surface of the fluid at the tip of the capillary tube elongates to form a conical shape known as the Taylor cone. With increasing field, a critical value is attained when the repulsive electrostatic force overcomes the surface tension and a charged jet of fluid is ejected from the tip of the Taylor cone. The discharged polymer solution jet undergoes a whipping process where in the solvent evaporates,

leaving behind a charged polymer fiber, which lays itself randomly on a grounded collecting metal screen. In the case of the melt the discharged jet solidifies when it travels in the air and is collected on the collector [13].

The coulombic repulsion force between charges of the same polarity produced in the polymer solution or melt by the emitting electrode destabilizes the hemi-spherical droplet of the polymer solution or melt located at the tip of the nozzle to finally form a droplet with a conical shape (i.e. the Taylor cone). With further increase in the electrostatic field strength beyond a critical value, the coulombic repulsion force finally exceeds that of the surface tension which results in the ejection of an electrically charged stream of the polymer solution or melts (the charged jet).

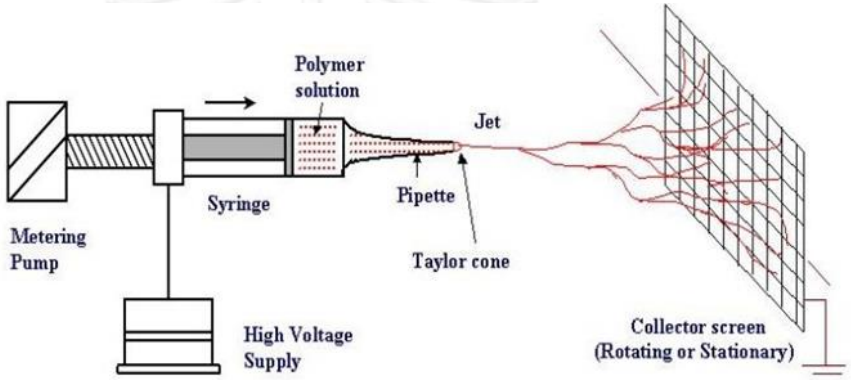

Fig. 2 Schematic diagram of electrospinning apparatus.

There are six major forces acting on an infinitesimal segment of the charged jet [14]:

1) Body or gravitational forces
2) Electrostatic forces which carry the charged jet from the nozzle to the target
3) Coulombic repulsion forces which try to push apart adjacent charge species present within the jet segment and are responsible for the stretching of the charged jet during its flight to the target
4) Viscoelastic forces which try to prevent the charged jet from being stretched
5) Surface tension which also acts against the stretching of the surface of the charged jet
6) Drag forces from the friction between the charged jet and the surrounding air

One of the most important quantities related with electrospinning is the fiber diameter. The fiber diameters will depend primarily on the jet sizes as well as on the polymer contents in the jets. It has been recognized that during the traveling of a solution extent is the applied electrical voltage. In general, a higher applied voltage ejects more fluid in a jet, resulting in a larger fiber diameter [15].

Another problem encountered in electrospinning is defects such as "beads" occur in polymer nanofibers. It has been found that the polymer concentration also affects the formation of the beads. In general, the higher polymer concentration results in fewer beads [16].

Fig. 3 SEM photographs of electrospun nanofibers from different polymer concentration solutions [17]

An addition of salts will result in a higher charge density on the surface of the solution jet during the electrospinning, bringing more electric charges to the jet. As the charges carried by the jet increased, higher elongation forces would be imposed to the jet under the electrical field, resulting in smaller bead and thinner fiber diameters [18].

2.1.2 Application of PAN nanofibers

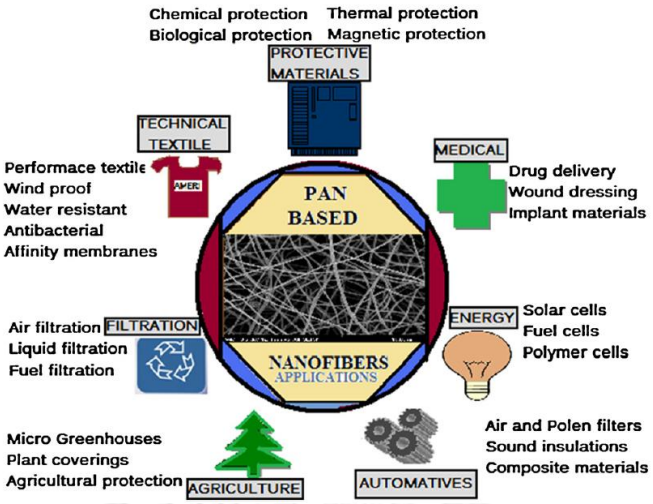

Fig. 4 Application of PAN nanofibers [19]

Filtration is needed in many engineering applications [20] due to the high surface area to volume makes a high surface adhesion. Particles smaller than 0.5 mm can adhere to the fibers used this filter is to filter and improve for the better [21, 22].

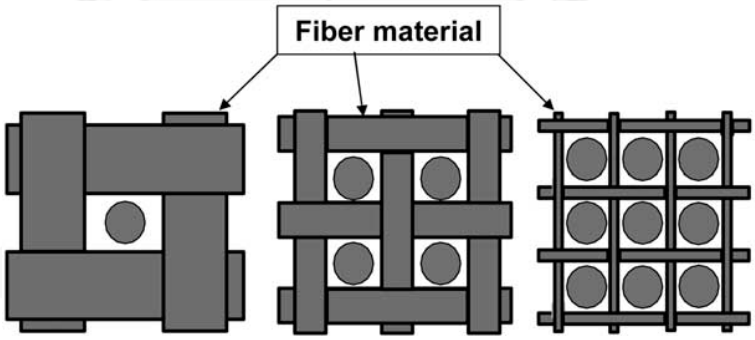

Fig. 5 The effect of the diameter of the fibers on the efficiency of the filter [23].

2.1.3 Carbon fiber production [24, 25]

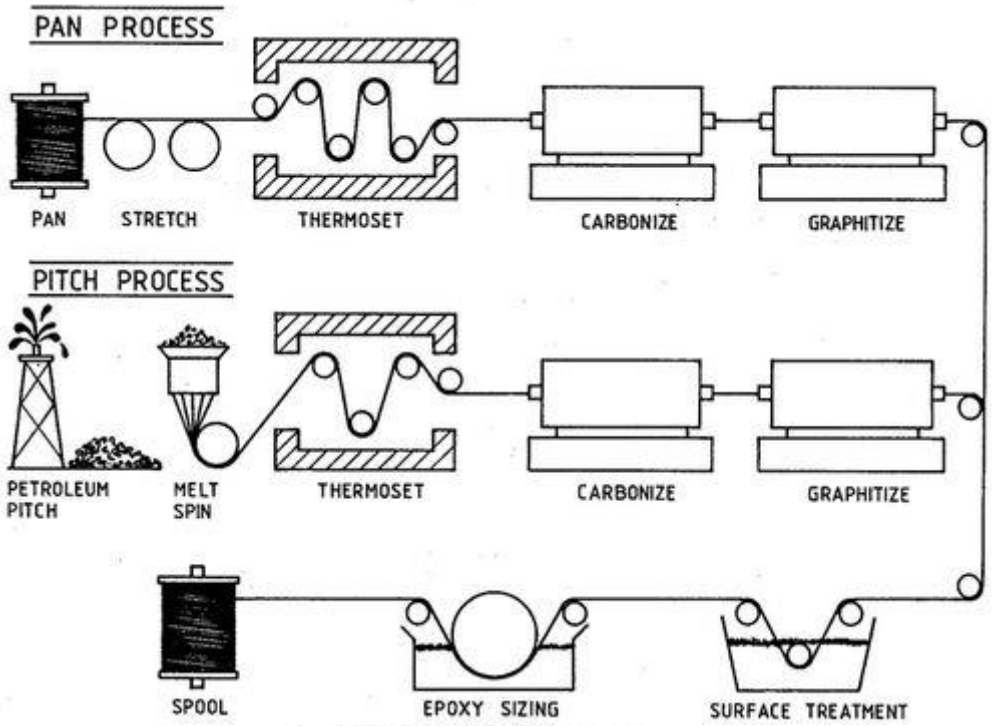

Fig. 6 Carbon fiber process from PAN

Carbon fibers were developed in the 1950s as reinforcement for high-temperature molded plastic components on missiles. The first fibers were manufactured by heating strands of rayon until they carbonized. This process proved to be inefficient, as the resulting fibers contained only about 20% carbon and had low strength and stiffness properties. In the early 1960s, a process was developed using polyacrylonitrile as a raw material. This produced a carbon fiber that contained about 55% carbon and had much better properties. The polyacrylonitrile conversion process quickly became the primary method for producing carbon fibers.

During the 1970s, experimental work to find alternative raw materials led to the introduction of carbon fibers made from a petroleum pitch derived from oil processing. These fibers contained about 85% carbon and had excellent flexural strength. Unfortunately, they had only limited compression strength and were not widely accepted.

Today, carbon fibers are an important part of many products, and new applications are being developed every year. The United States, Japan, and Western Europe are the leading producers of carbon fibers.

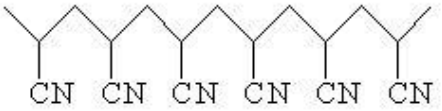

Fig. 7 PAN molecule

2.1.3.1 Stabilizing. Before the fibers are carbonized, they need to be chemically altered to convert their linear atomic bonding to a more thermally stable ladder bonding. This is accomplished by heating the fibers in air to about 390-590 °F (200-300 °C) for 30-120 minutes. This causes the fibers to pick up oxygen molecules from the air and rearrange their atomic bonding pattern. The stabilizing chemical reactions are complex and involve several steps, some of which occur simultaneously. They also generate their own heat, which must be controlled to avoid overheating the fibers. Commercially, the stabilization process uses a variety of equipment and techniques. In some processes, the fibers are drawn through a series of heated chambers. In others, the fibers pass over hot rollers and through beds of loose materials held in suspension by a flow of hot air. Some processes use heated air mixed with certain gases that chemically accelerate the stabilization.

2.1.3.2 Carbonizing. Once the fibers are stabilized, they are heated to a temperature of about 1,830-5,500 °F (1,000-3,000 °C) for several minutes in a furnace filled with a gas mixture that does not contain oxygen. The lack of oxygen prevents the fibers from burning in the very high temperatures. The gas pressure inside the furnace is kept higher than the outside air pressure and the points where the fibers enter and exit the furnace are sealed to keep oxygen from entering. As the fibers are heated, they begin to lose their non-carbon atoms, plus a few carbon atoms, in the form of various gases including water vapor, ammonia, carbon monoxide, carbon dioxide, hydrogen, nitrogen, and others. As the non-carbon atoms are expelled, the remaining carbon atoms form tightly bonded carbon crystals that are aligned more or less parallel to the long axis of the fiber. In some processes, two furnaces operating at two different temperatures are used to better control the rate de heating during carbonization.

2.1.3.3 Treating the surface. After carbonizing, the fibers have a surface that does not bond well with the epoxies and other materials used in composite materials. To give the fibers better bonding properties, their surface is slightly oxidized. The addition of oxygen atoms to the surface provides better chemical bonding properties and also etches and roughens the surface for better mechanical bonding properties. Oxidation can be achieved by immersing the fibers in various

gases such as air, carbon dioxide, or ozone; or in various liquids such as sodium hypochlorite or nitric acid. The fibers can also be coated electrolytically by making the fibers the positive terminal in a bath filled with various electrically conductive materials. The surface treatment process must be carefully controlled to avoid forming tiny surface defects, such as pits, which could cause fiber failure.

2.1.3.4 Sizing. After the surface treatment, the fibers are coated to protect them from damage during winding or weaving. This process is called sizing. Coating materials are chosen to be compatible with the adhesive used to form composite materials. Typical coating materials include epoxy, polyester, nylon, urethane, and others. The coated fibers are wound onto cylinders called bobbins. The bobbins are loaded into a spinning machine and the fibers are twisted into yarns of various sizes.

2.2 Porosity and sorption behavior [26, 27]

2.2.1 Principles of Adsorption

The term adsorption is said to have been first used by Kayser [28] in 1881 in order to explain the condensation of gases on surfaces, in contrast to gas absorption in which gas molecules penetrate the bulk phase of the absorbing solid. The term ‘sorption’ was proposed by McBain [29] as a complete description of mass transport into a solid, encompassing surface adsorption, absorption by penetration into the solid and condensation within pores.

Adsorption is described as the enrichment of one or more components in the interfacial layer, [30] i.e. an excess of molecules exists at the adsorbate/adsorbent interface, upon exposure of an adsorbing solid to a gas or vapor. It is the selective collection and concentration onto solid surfaces of certain molecules contained in a vapor or gas stream. Hence, vapors or gases referred to as adsorbates when adsorbed, even of mixed systems and at low concentrations, may be captured, often selectively, and removed from the effluent stream using a material of the category of adsorbents.

Adsorption is divided into the two sub-categories of physical adsorption (physisorption) or van der Waals adsorption and chemical adsorption (chemisorption) and the adsorption process can be determined whether chemical bonds are formed during the process. Physisorption is applicable to all adsorbate-adsorbent systems

provided the conditions of pressure and temperature are suitable whereas chemisorption may only occur if the system is capable of making a chemical bond.

2.2.2 Physical Adsorption (Physisorption)

The process is a dynamic one where an equilibrium state exists with molecules and the interaction between the adsorbate and adsorbent.

No chemical bonds are formed during physical adsorption; attraction between the adsorbate and adsorbent exists by the formation of intermolecular electrostatic, such as London dispersion forces, or van der Waals forces from induced dipole-dipole interactions, or may be dependent on the physical configuration of the adsorbent such as the porosity of activated carbons. Dispersion forces are the result of rapid fluctuations in the electronic density of one adsorbent molecule inducing an electrical moment in a second atom [27]. If the adsorbate possesses a permanent dipole, or even a multipole, then additional interactions may occur, as charge distributions are induced in the adsorbent and interactions of these moments with any permanent field of the solid.

The process is a very general one and is analogous with that of condensation. Physisorption occurs to varying extents for all adsorbates, gases and vapours, with all adsorbing solids and the effect increases with decreasing temperature or increasing pressure. Physical adsorption is based on certain basic considerations and adsorption on a heterogeneous surface, that is a surface on which the sites are different, occurs at the sites of highest adsorption potential. The process of physical adsorption into the microporous structure of activated carbon follows the theory of Dubinin [31-33].

The mechanism of adsorption is dependent upon the size of the admolecule in comparison with the pore width due to the energetic interactions between the chosen adsorbate and the pores. Admolecules initially adsorb into the pores with the highest energy, ignoring activated diffusion effects, then adsorption proceeds via filling of progressively larger, or decreasing energy, porosity. Some pores are capable of accommodating two or three admolecules and, therefore, may undergo co-operative adsorption effects by reducing the volume element thus increasing the energy and adsorptive potential of the pore.

The process of adsorption is always exothermic due to the increased ordering of the adsorbate on the adsorbent surface, reducing the entropy, as:

$$\Delta G = \Delta H - T\Delta S$$

Thus the amount adsorbed should decrease with increasing temperature as a reduction in the thermal energy supplied to the process, by Le Chatelier's principle, favours the exothermic process of adsorption increasing the equilibrium uptake, except in the case of activated diffusion.

It has been proposed by Lamond and Marsh, [34] by the interpretation of data for physical adsorption of nitrogen on both polar and non-polar surfaces that physical adsorption is independent of the surface chemistry of the adsorbent.

2.2.3 Chemical Adsorption (Chemisorption)

Chemisorption involves the transfer of electrons between the adsorbent and the adsorbate with the formation of chemical bonds, by chemical reaction, between the two species causing adhesion of the adsorbate molecules. Chemical adsorption is far less common than physical adsorption and due to the chemical bonds formed regeneration of the adsorbent for subsequent re-use is often difficult or impossible [35].

Due to the fact that chemical bonds are formed during the adsorption process, desorption of the adsorbed phase may yield products which are chemically different to the original adsorbate. For example oxygen may chemically bond to the surface of a carbon, which upon desorption may evolve CO and CO_2 as products.

Table 1 Characteristics Associated with Physical/Chemical Adsorption [36]

Details	Physical Adsorption	Chemical Adsorption
Heat of Adsorption/kJmol^{-1}	20 - 40 c.f. heats of liquefaction	80 c.f. bulk-phase chemical reactions
Rate of Adsorption (at 273 K)	Fast	Slow
Temperature Dependence of Uptake (with Increasing T)	Decreases	Increases
Desorption	Easy- by reduced pressure or increased temperature	Difficult - high temperature required to break bonds
Desorbed Species	Adsorbate unchanged	May be different to original adsorptive
Specificity	Non-specific	Very Specific
Monolayer Coverage	Mono or multilayer condition dependent	Monolayer

2.2.4 Porosity

The word pore comes from the Greek word ‘poros’ which means passage. This indicates the role of a pore acting as a passage between the external and the internal surfaces of a solid, allowing material, such as gases and vapors, to pass into, through or out of the solid. Almost all adsorbents that are used in catalysis or for purification/separation purposes possess porosity, and this is the only practical method of introducing greatly enhanced surface areas into a solid.

Activated carbons were the source of several observations made by Bussy. [33] He reported that porosity, although he could not measure it directly, was extremely important and that the decolorizing power of a carbon was dependent on the parent precursor and the processes used in its manufacture.

Porosity has been studied extensively by the process of adsorption [27] where exposure of a porous solid to an adsorbate creates a concentration of the adsorbate at the surface, within molecular or atomic distance, greater than the adsorptive concentration in the gas phase. An excess of molecules exists dynamically at the interface in the process called adsorption.

There are four terms generally used to describe the accessibility of porosity:

‘Open pore’ - a pore which is connected to the external surface of a solid and allows the passage of an adsorbate through the solid

‘Closed pore’ - a void within the solid which is not connected to the external surface and hence is isolated

‘Transport pores’ - these connect different parts of the external surface of the solid to the inner microporosity

‘Blind pores’ - are connected to transport pores but do not lead to any other pore or surface

It may be useful to explain the terms of internal and external surfaces:

‘Internal surface’ - composed of the area which surrounds the closed pores as well as all fissures and cracks which penetrate deeply into the interior of the adsorbent which are deeper than they are wide, and

‘External surface’ - consists of the protrusions and superficial cracks which are wider than they are deep.

The total surface of a carbon material is predominantly composed of internal surface and activated carbons owe their adsorptive properties to the internal surface area and pore size distribution with the external surface area and functional groups playing a comparatively minor role [37].

Fig. 8 below shows the different components of a typical mass transport system of a solid. The total pore volume is essentially the sum of two fractions:

$$Vt = Vo + Vc$$

where Vt is the total pore volume, Vo is the pore volume due to the open porosity in the solid, including transport and blind pores, and Vc is the closed pore volume.

Fig. 8 Different types of porosity

The total pore volume of a carbon is independent of the adsorbate, provided the amount adsorbed is expressed as a liquid volume and excluding selective effects, according to the Gurvitsch rule. An exception to this rule is water as it is assumed that water molecules cannot hydrogen bond effectively in the narrow micropores effectively reducing the density of the adsorbed phase hence reducing the pore volume. Unfortunately this rule does not take size exclusion effects into account as is often the case with CMS but it can be assumed that this rule is applicable ignoring all other effects.

2.2.5 Classification of pores

Porosity has a classification system as defined by IUPAC, [38] which gives a guideline of pore widths applicable to all forms of porosity. Distinctions in porosity class are not rigorous and they may often overlap in size and definition. The widely accepted I.U.P.A.C. classification is as follows:

Table 2 Classification of pores according to their width

	Width
Micropores	Less than ~ 20 Å (2 nm)
Mesopores	Between ~ 20 and ~ 500 Å (2 and 50 nm)
Macropores	More than ~ 500 Å (50 nm)

2.2.6 Pore Size Distribution

The distribution of pore sizes may be described in terms of micro-, meso- and macropores but are not necessarily tri-modal, exhibiting three peaks of varying ratios, and this result formed the basis of Dubinin's classification [39].

A complete distribution is not always present in a carbon and some species may exhibit only some types of porosity. Distinct peaks are not always observed and some systems exhibit wide distributions over all pore diameters or a constant decrease/increase in pore frequency with variation in pore diameter.

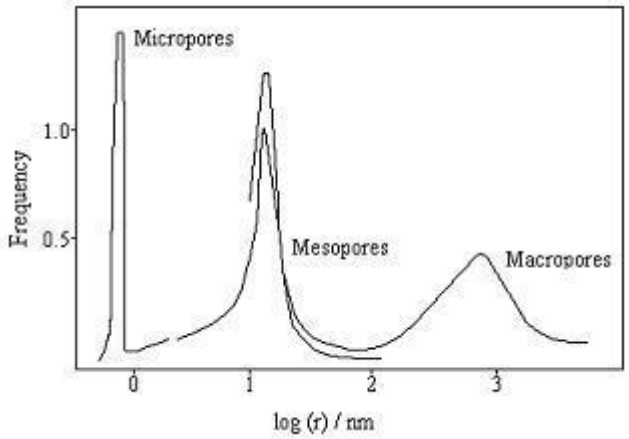

Fig. 9 Schematic of the tri-modal pore-size distribution found in many carbons.

2.2.7 Classification of Adsorption Isotherms

Adsorption isotherms should conventionally be plotted on the basis of relative pressure, p/p_o (x-axis) versus amount adsorbed expressed as a molar quantity (y-axis) in $mmolg^{-1}$, to allow comparisons to be made. The experimental procedure involves the use of partial pressure, where the actual pressure is expressed with respect to the saturation vapor pressure at a constant temperature of adsorption, hence the process is isothermal. Adsorption data may alternatively be expressed in terms of an isobar, the variation in uptake with temperature at constant pressure, the change in temperature with pressure at a constant surface coverage. Isotherms provide a significant amount of information about the adsorbent used and the interaction with the adsorbate in the system, including:

i) Assessment of the surface chemistry and fundamentals involved in the adsorption process
ii) Estimates of the surface area, pore volume and pore size distribution
iii) Efficiency profiles for carbons used in industrial processes.

The interpretation of adsorption isotherms can yield a large amount of information about the processes involved, as outlined above, but this is only possible upon careful analysis of the data obtained and this can often lead to confusion in the interpretations made. An understanding of the adsorption mechanisms involved in the different classes of porosity is essential to explain the shapes observed.

The extent of adsorption on a surface, usually denoted n, is generally a function of the temperature, pressure and nature of the adsorbent and adsorbate:

$$n = f(P, T, \text{adsorbate, adsorbent})$$

For isothermal adsorption of a particular system this simplifies to

$$n = f(P)T, \text{adsorbent, adsorbate}$$

By working within the limits of vacuum and the saturation vapor pressure, the pressure may be expressed in terms of relative vapor pressures, i.e. p/p_o:

$$n = f(p/p_o)T, \text{adsorbent, adsorbate}$$

This gives a universal basis upon which all isotherms may be displayed in order to make the comparison of results easier. The above relationship may be used to graphically represent uptake profiles in the form of an 'adsorption isotherm'.

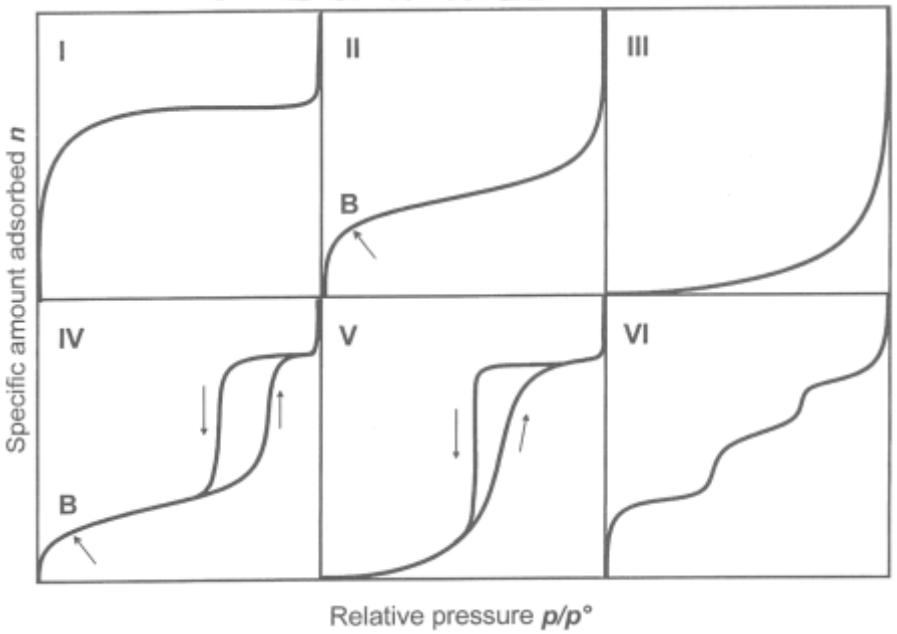

Fig. 10 Diagrammatic representation of isotherm classification

All adsorption isotherms should fit at least one, or at least a combination of two or more, of the six recognized types classified by Brunauer, Deming, Deming and Teller [40] (B.D.D.T. system). The figure above shows the possible shapes and information which may be drawn from them is outlined below:

Type I Isotherm - these are typical of adsorbents with a predominantly microporous structure, as the majority of micropore filling will occur at relative pressures below 0.1. The adsorption process is usually complete at a partial pressure of ~0.5. Examples include the adsorption of nitrogen on carbon at 77K and ammonia on charcoal at 273 K.

Type II Isotherm - physical adsorption of gases by non-porous solids is typified by this class of isotherm. Monolayer coverage is followed by multilayering at high relative pressures. Carbons with mixed micro- and meso-porosity produce Type II isotherms.

Type III Isotherm - the plot obtained is convex to the relative pressure axis. This class of isotherm is characteristic of weak adsorbate-adsorbent interactions [41] and is most commonly associated with both non-porous and microporous adsorbents. The weak interactions between the adsorbate and the adsorbent lead to low uptakes at low relative pressures. However, once a molecule has become adsorbed at a primary adsorption site, the adsorbate-adsorbate interaction, which is much stronger, becomes the driving force of the adsorption process, resulting in accelerated uptakes at higher relative pressure. This co-operative type of adsorption at high partial pressures is known as cluster theory and examples include the adsorption of water molecules on carbon where the primary adsorption sites are oxygen based.

Type IV Isotherm - A hysteresis loop, which is commonly associated with the presence of mesoporosity, is a common feature of Type IV isotherms, the shape of which is unique to each adsorption system. Capillary condensation gives rise to a hysteresis loop [42] and these isotherms also exhibit a limited uptake at high relative pressures.

Type V Isotherm - these isotherms are convex to the relative pressure axis and are characteristic of weak adsorbate-adsorbent interactions [41]. These isotherms are indicative of microporous or mesoporous solids. The reasons behind the shape of this class of isotherm are the same as those for Type III and again water adsorption on carbon may exhibit a Type V isotherm.

Type VI Isotherm - introduced primarily as a hypothetical isotherm, the shape is due to the complete formation of monomolecular layers before progression to a subsequent layer. It has been proposed, by Halsey, [43] that the isotherms arise from adsorption on extremely homogeneous, non-porous surfaces where the monolayer capacity corresponds to the step height. One example known to exist is the adsorption of krypton on carbon black (graphitized at 3000 K) at 90 K [44].

2.3 Literature reviews

Many researchers have researched and developed on the carbon nanofibers were used as adsorbents of volatile organic compounds (VOCs) by focusing on benzene, toluene and xylene (BTX), which are compounds VOCs, are very common in the atmosphere and most harm to humans.

In choosing the right material for use as a sorbent for organic compounds, *Jahangiri M. et al. [9]* have studied the adsorption of BTX by comparing their adsorption ability from different type of adsorbents are Multi-walled carbon nanotubes (MWNT), Single-walled carbon nanotubes (SWNT), Double-walled carbon nanotubes (DWNT), Carbon nanofibers (CNF), Nanoporous carbon (NC), MWNT-COOH and activated carbon showed that CNF can absorb highest volume of BTX followed by SWCNT, MWNT, NC, and MWNT-COOH, respectively. Factors affecting adsorption characteristics of organic material are porous, surface area, surface defects, and functional groups. Which the investigators have observed that carbon structural nanoparticles can absorb BTX over activated carbon except MWNT-COOH. In addition *J.W. Park et al. [45]* have researched to find out the disadvantages of activated carbon are flammable, hard to regenerate, and need to control humidity. But for activated carbon fiber (ACF) that are uniform in size and dimension can absorb substances in more quantities. The rate of adsorption and desorption of adsorption on activated carbon faster and easier to manage. The popular materials used in making ACF include Pitch, Cellulose, Polyacrylonitrile and Phenol resins, which the researchers have used Pitch-based activated carbon fiber with a BET surface area was 764.3 m^2/g to study toluene, dichloromethane, and trichloroethylene equilibrium adsorption. The results of the experiments are associated with isometric terminal adsorption of Toth equation.

For application of electrospinning process to fabricate nanofibers, many researchers have studied several polymers type as carbon source. *Tamer U. et al. [46]* used polymethylmethacrylate mixed with beta-cyclodextrin to fabricated nanofibers to trap the substance of aniline, styrene, and toluene, which shows that the nanofibers with cyclodextrin functional groups can be used as a filter for the nanofibers developed for the treatment of organic vapors. *H. Katepalli et al. [10]* have studied to prepare carbon nanofibers made from PAN by spinning fibers onto woven carbon microfibers (ACF-PAN) and PAN prepared by base metals (ACF-CNF) was used as absorbents for pollutants in the atmosphere compared to carbon microfibers. The results show stabilized ACF-PAN was effective in absorbing toluene best. Because more volume of porous in micron range, more pore volume can

absorbing more and faster. It also has a greater specific surface area (BET surface area was 1,303 m^2/g)

CHAPTER 3
EXPERIMENTAL PROCEDURE

3.1 Test Materials and Chemicals

The specification of test materials and chemicals used in this research work were shown in **Table 3**

Table 3 The specifications of test materials and chemicals

Type	Usage	Purity / Grade
Polyacrylonitrile (s)	Polymer source	Analytical grade
N,N-Dimethylformamide	Solvent for PAN solution	Analytical grade
Manganese (II) acetate tetrahydrate	Mn precursor	Analytical grade
Toluene	Adsorbate	Analytical grade
Ethylene glycol	Solvent for toluene	Analytical grade
Air (g)	Carrier gas for stabilization	Atmospheric air
Nitrogen (g)	Carrier gas to tube furnace	UHP* 99.999 % min
Nitrogen (g)	Carrier gas for GC	UHP* 99.999 % min
Hydrogen (g)	For flame ignition	HP* 99.99 %
Air zero (g)	For flame ignition	HP* 99.995 %
Air zero (g)	Carrier gas for toluene vapor to tube adsorber	HP* 99.995 %
Quartz wool	Support adsorbate	GC grade

* UHP = Ultra high purity and HP = High purity

The well-known advantage of changing from activated carbon to activated carbon nanofibers as an adsorbent for toluene adsorption such as high specific surface area with high microporous and lightweight, could improve adsorption capacity, or maybe increase adsorption rate, especially in case of low adsorbate concentration.

This research aims to prepare ACNFs from PAN nanofibers fabricated by electrospinning process will be investigate effect of various PAN concentration and carbonization temperature for improve pore characteristics such as specific surface area and micropore volume to use as adsorbent for toluene adsorption. For others factor that affect the electrospining process such as distance between the capillary tip and collection screen, electric potential will be fixed, due to those factor affect only fibers diameter.

3.2 Preparation of Activated Carbon Nanofibers

3.2.1 Formation of PAN nanofibers

Concentrations of PAN solution have varied from 5 wt.%, 8 wt.%, 10 wt.% to 12 wt.% PAN in DMF. For 5 and 12 wt.% PAN in DMF were not suitable for polymer source due to inappropriate viscosity of polymer solution. Low viscosity of PAN solution could not spin to fibers and has a droplet of solution onto the aluminum collector and onto the floor as 5 wt.% PAN in DMF while high viscosity of PAN solution could not spin to fibers also because of electrostatic force not overcome surface tension of polymer solution make the dried solid deposited onto aluminum collector as 12 wt. % PAN in DMF. Hence, the suitable concentrations for varying in this research were 8 and 10 wt. % PAN in DMF.

A solution containing 8 and 10 wt.% PAN and 1 wt.% manganese (II) acetate tetrahydrate in DMF was prepared and stirred at room temperature for 1 hr. The homogeneous solution was transferred to a 30 mL glass syringe with 1.1 mm diameter metal needle.

Fig. 2 shows the experiment apparatus for the electrospinning process. A DC power supply (Gamma high voltage research, USA.) was used to control high voltage supplied for the electrospinning process. The anode of the power supply was clamped to a syringe needle tip, and the cathode was connected to a stationary aluminum collector. Upon the application of high potential of 20 kV across the 18 cm distance between the tip of the needle and the aluminum collector [11], the

solution in the syringe was ejected as a jet toward the collector. As the solvent evaporated, PAN nanofibers were formed on the collector.

3.2.2 Stabilization

The electrospun fibers were stabilized by heating to 280 ℃ at the heating rate of 1 ℃/min in air, and held at that temperature for 1 hr. [11] in order to oxidized polymer molecules with oxygen. Consequently, the structure of the PAN changes from a long aliphatic chain molecule into chain of molecular rings and eliminated organic impurities.

3.2.3 Carbonization

The stabilized fibers were then carbonized by heating to temperature in the various range of 800, 900, and 1,000 ℃ at the rate of 5 ℃/min under nitrogen atmosphere and held at that temperature for 1 hr [11] in tube furnace in order to eliminate various non-carbon impurities. After the carbonization, the remaining carbons were bonded strongly.

3.2.4 Activation

The carbonized fibers were then activated at 800 ℃ in tube furnace by gas mixture of steam boiled at 100 ℃ and nitrogen for 30 min to prevent mesopore formation.

3.3 Characterization of Activated Carbon Nanofibers

3.3.1 Scanning electron microscopy (SEM) and Scanning Electron Microscopy with X-ray microanalysis (SEM-EDS)

Morphology, diameter and element content of the ACNFs were observed on JSM-6400 scanning electron microscope. The SEM was operated using the secondary electron mode at 15 kV at the Scientific and Technological Research Equipment Center (STREC), Chulalonkorn University.

Fig. 11 Scanning electron microscopy (SEM, JSM-6400)

3.3.2 Fourier transform infrared spectroscopy (FTIR)

Functional groups of the ACNFs were identified by using an infrared spectroscopy (Nicolet 6700, Thermo Scientific). Sample preparation was done before measurement by mixed ACNFs with Potassium bromide (KBr) and compressed into thin pellet with carefully.

Fig. 12 Fourier transform infrared spectroscopy (FTIR, Nicolet 6700)

3.3.3 Automatic specific surface area/pore size distribution measurement.

Specific surface area, total pore volume, micropore volume, and mean pore diameter were characterized by nitrogen (N_2) adsorption isotherm at 77 K via the Brunauer, Emmett, and Teller (BET) equation by the single point method (BELSORP-mini II, BEL JAPAN INC).

Fig. 13 Automatic specific surface area/pore size distribution measurement (BELSORP-mini II, BEL JAPAN INC).

3.3.4 Thermogravimetric Analysis

The weight loss of toluene on ACNFs after adsorbed was estimated by Thermogravimetric analysis (TGA/DSC1 Thermogravimetric Analyzer, Mettler Toledo).

Fig. 14 TGA/DSC1 Thermogravimetric Analyzer, Mettler Toledo

3.4 Toluene Adsorption Process

Dynamic breakthrough tests were carried out by flowing toluene vapor mixture through an adsorption tube. The inner diameter is 7 mm and control temperature about 30 °C. The flow rate of zero air was 2.50 ml/min. Before flowing toluene vapor mixture through adsorption tube, toluene vapor was equilibrated with passing zero air for 1.5 hr. The equilibrated toluene with zero air mixture was flows through the copper tube contain ACNFs and commercial activated carbon sample inside. Amount of ACNFs and commercial activated carbon was packed in adsorption about 0.02 g covered with quartz wool at inlet and outlet side to support and hold the adsorbent. The inlet toluene in zero air balance concentration will be measured. The toluene standard gas is controlled quantitatively by mass flow controller (MFC), and the amount of toluene adsorption is investigated by gas chromatography (GC-14B, SHIMAZSU) until it breakthrough. The amount of toluene calculated from toluene calibration curve.

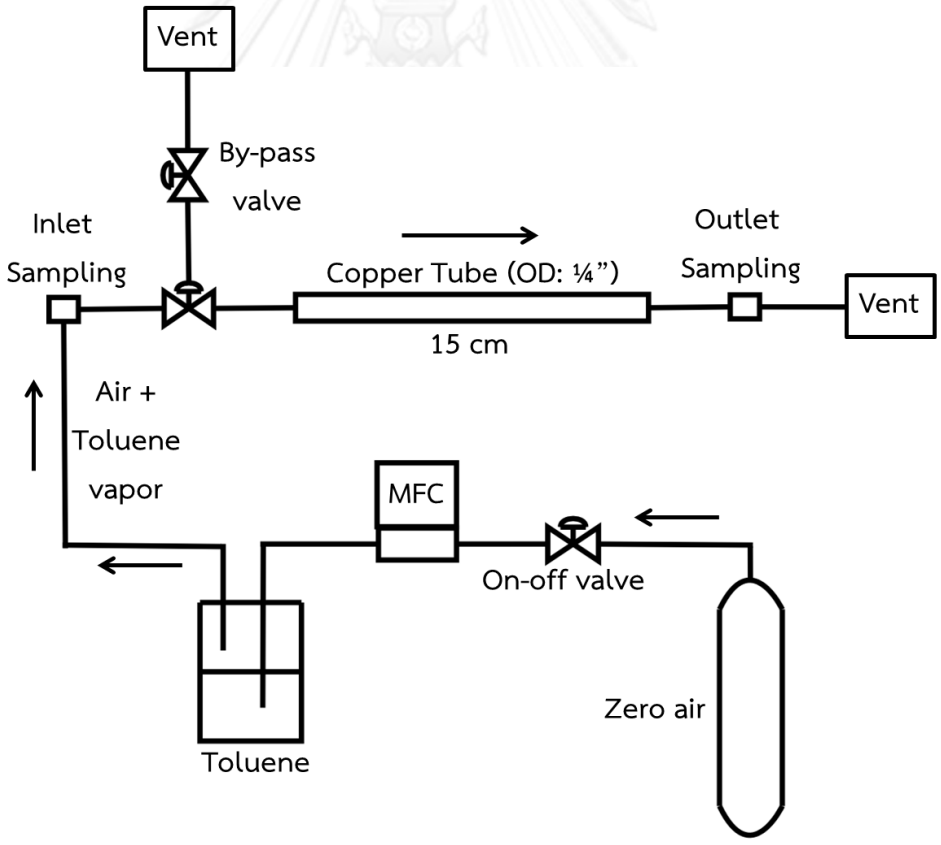

Fig. 15 The adsorption apparatus for studies the toluene adsorption test.

Fig. 16 Gas chromatography (GC-14B, SHIMAZSU)

CHAPTER 4
RESULTS AND DISCUSSION

4.1 Formation of PAN nanofibers

After prepared PAN nanofibers by electrospinning process by varying concentration from 5 wt. %, 8 wt. %, 10 wt. % and 12 wt. % PAN in DMF, to find two appropriate concentrations to prepared ACNFs from SEM images as bellows.

Fig. 17 shows SEM images of PAN fibers formed from 5 wt. %, 8 wt. %, 10 wt. % and 12 wt. % PAN in DMF. PAN nanofibers formed from 5 wt. % PAN in DMF has low viscosity can cause bead formation and non-uniform fibers diameter with average diameter is 102 nm (**Fig. 17 (a)**). The formation of the beaded nanofibers can be considered as the capillary breakup of the electrospinning jets by surface tension, altered by the presence of electrical forces [47]. While PAN nanofibers formed from 8 and 10 wt. % PAN in DMF have a uniform fibers diameter as well with average diameter are 264 and 427 nm (**Fig. 17 (b), (c)**), respectively. Meanwhile, PAN fibers formed from 12 wt. % PAN in DMF (**Fig. 17 (d)**) has high viscosity which electrostatic force could not carry the charged jet to the collector cause of this PAN solution has high viscoelastic force to prevent the charged jet from being stretched, its make a very large and non-uniform diameter with average diameter is 1,969 nm or 1.97 micron.

Hence, the suitable PAN concentrations for prepare ACNFs in this selected electrospinning conditions are 8 wt. % and 10 wt. % PAN in DMF.

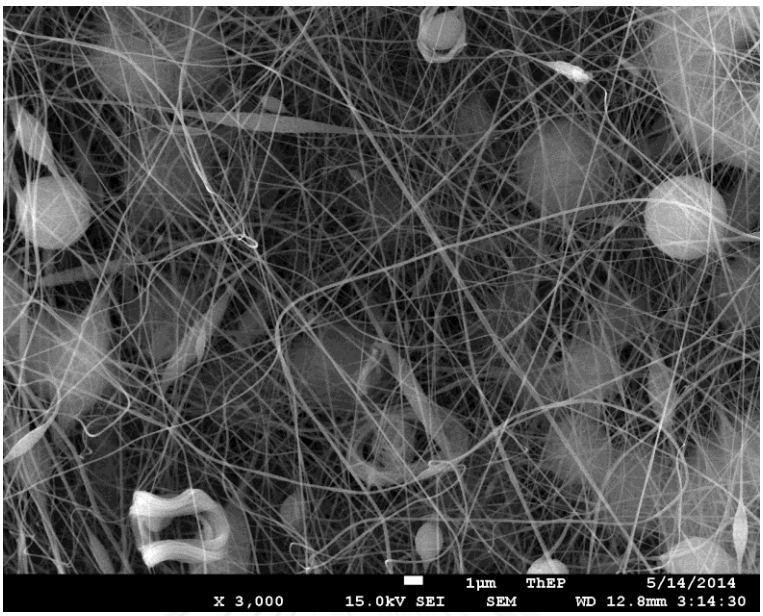

Fig. 17 (a) PAN fibers formed from 5 wt. % PAN in DMF

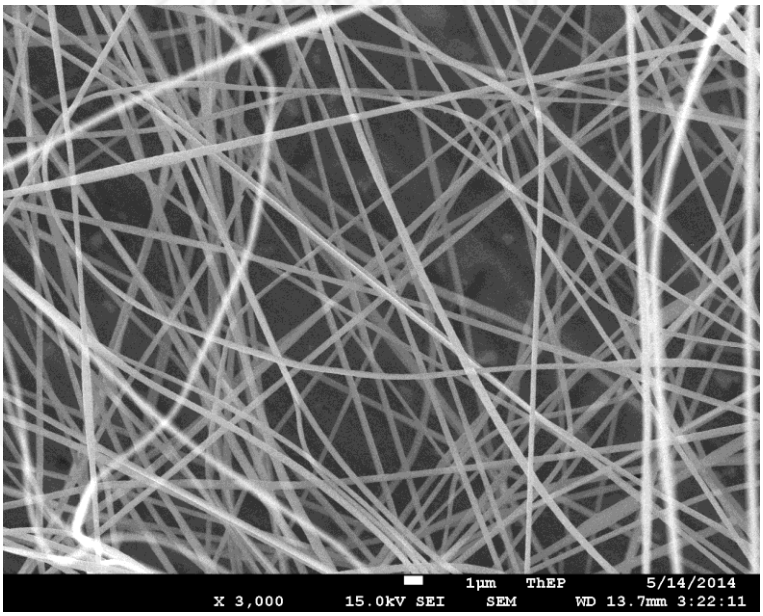

Fig. 17 (b) PAN fibers formed from 8 wt. % PAN in DMF

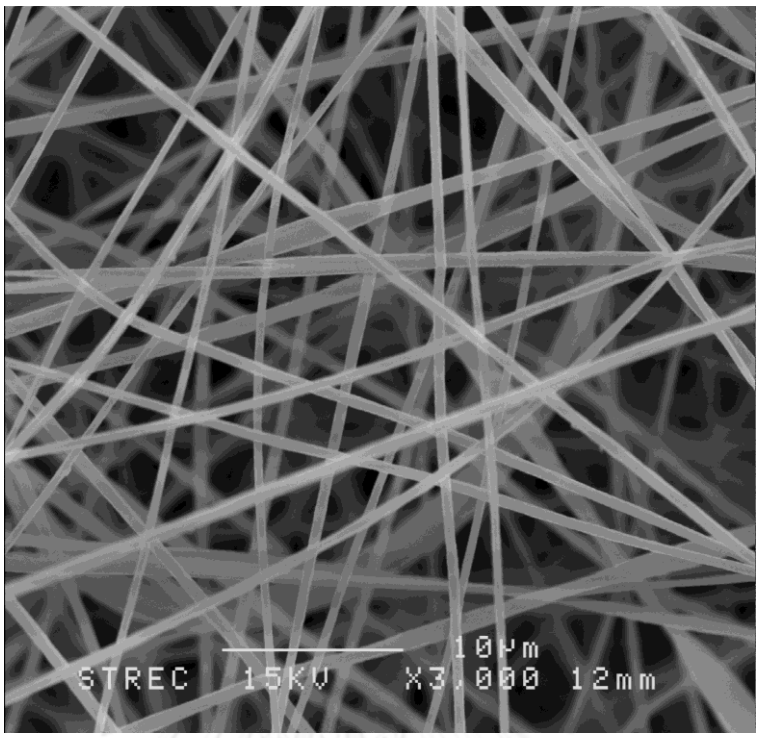

Fig. 17 (c) PAN fibers formed from 10 wt. % PAN in DMF

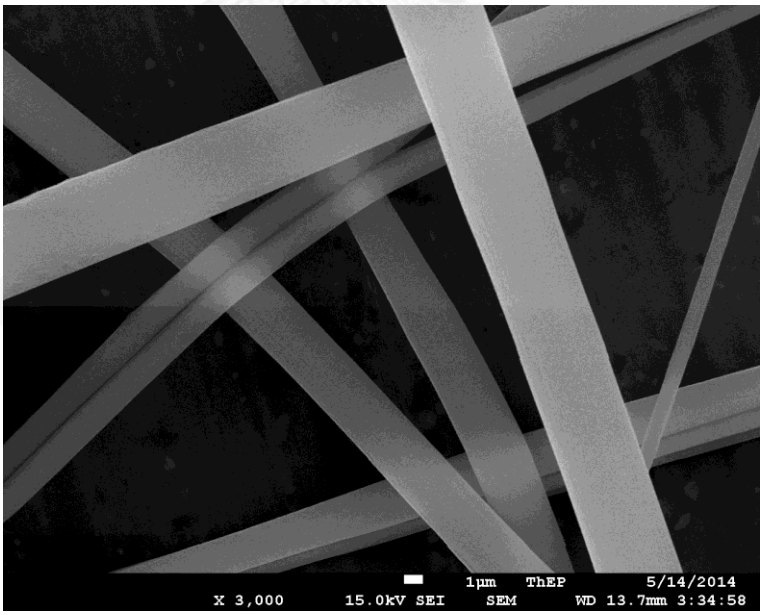

Fig. 17 (d) PAN fibers formed from 12 wt. % PAN in DMF

In addition, the diameter of PAN nanofibers from varying of PAN concentration in DMF shows in **Fig. 18**, higher concentration of PAN in DMF with higher viscosity of solution will fabricated larger fibers diameter with large distribution of fiber diameter.

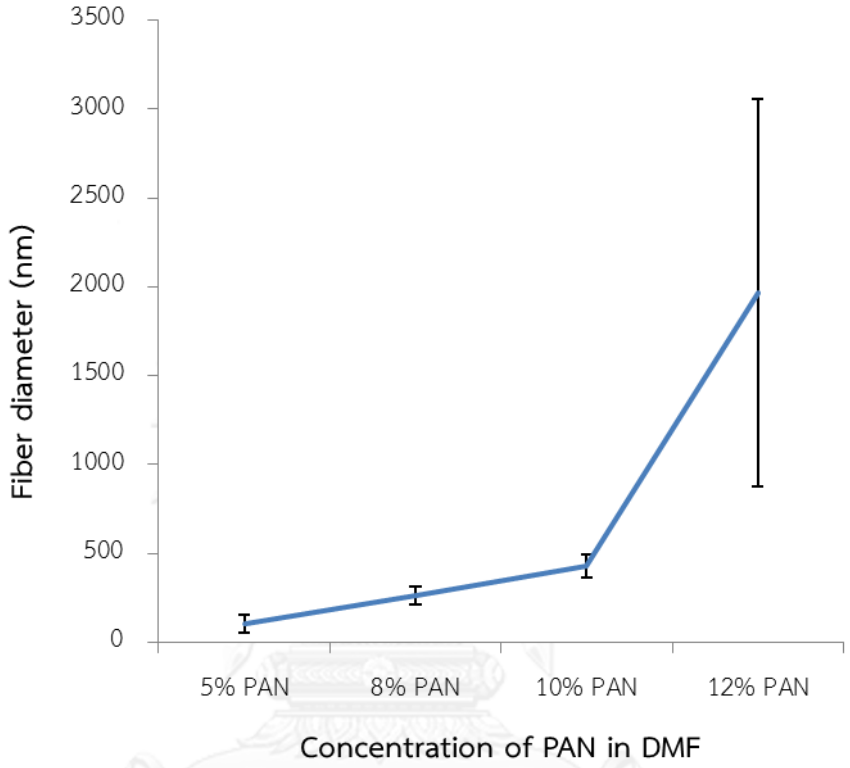

Fig. 18 shows relativity of concentration of PAN in DMF and fiber diameter

Fig. 19 shows SEM images of PAN fibers formed from 8 wt. % PAN with 1 wt.% Mn (Fig. 19a), PAN fibers formed from 10 wt. % PAN solution without Mn (Fig. 19b) and PAN fibers formed from 10 wt. % PAN solution with 1 wt. % Mn (Fig. 19c), respectively. All obtained products are smooth fibers with uniform diameter. Hence, the conditions of electrospinning process as above can produce PAN nanofibers. The average diameter of the fibers formed from the solution with 8 and 10 wt.% PAN with 1 wt. % Mn is 240 and 400 nm, respectively. In addition, fibers formed from 8 wt.% PAN solution with 1 wt.% Mn have a smaller diameter than 10 wt.% PAN solution cause of lower viscous polymer solution have the higher surface tension of solution make more fine jet of polymer solution from needle tip during electrospinning process. In addition, **Fig. 20** shows Mn-embedded PAN fibers has a smaller diameter than pure PAN fibers cause of Manganese in PAN can enhance electricity conductivity of solution make more fine jet of PAN solution to collector.

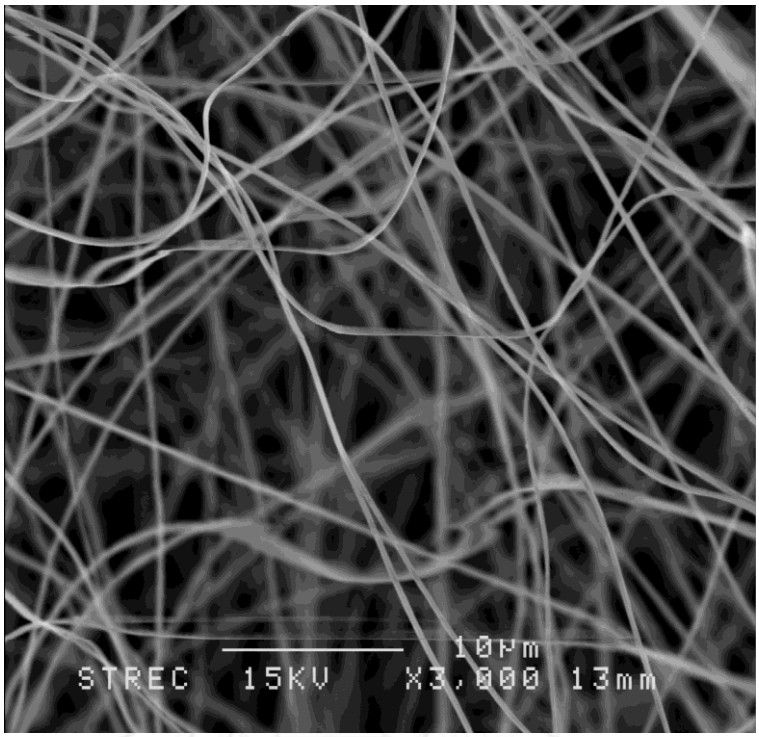

Fig. 19 (a) SEM of PAN fibers formed from 8 wt. % PAN solution with 1 wt. % Mn

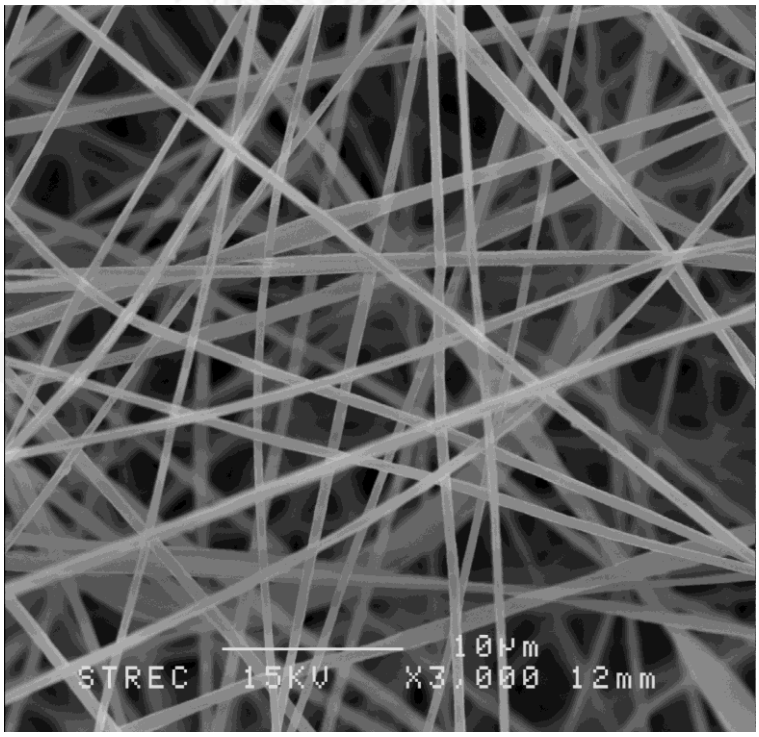

Fig. 19 (b) SEM of PAN fibers formed from 10 wt. % PAN without manganese

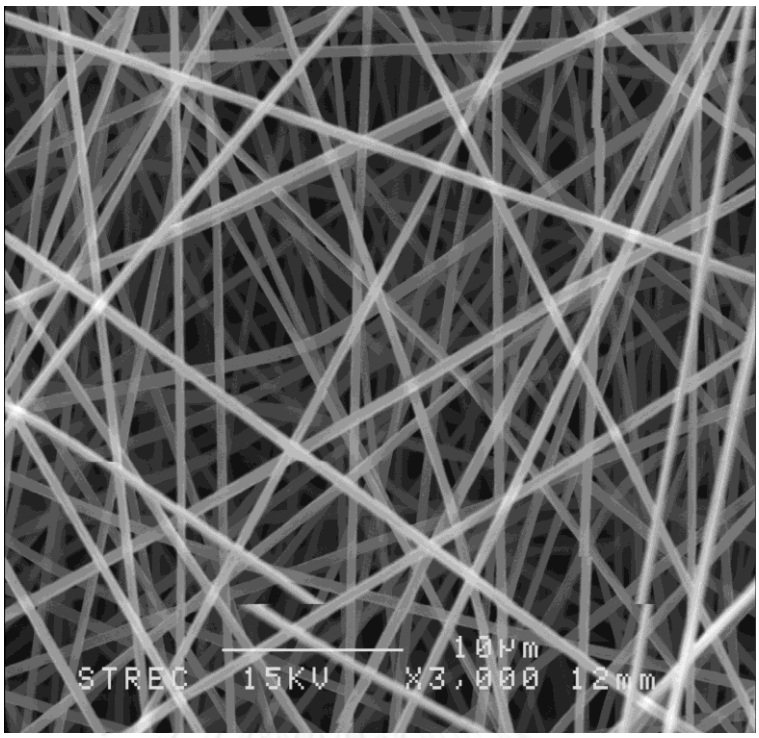

Fig. 19 (c) SEM of PAN fibers formed from 10 wt.% PAN solution with 1 wt.% Mn

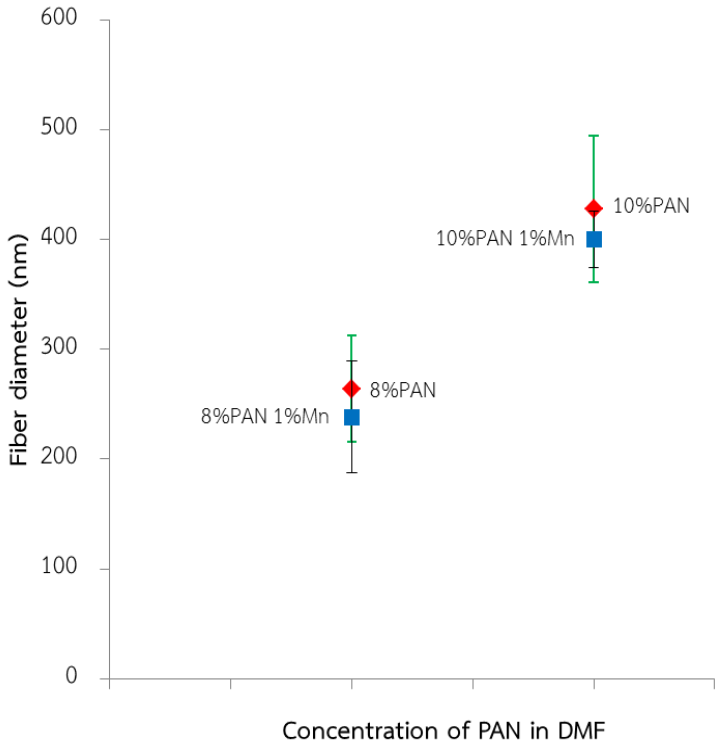

Fig. 20 shows relativity of concentration of PAN in DMF with and without Mn and fiber diameter

4.2 Characterization of ACNFs

4.2.1 Morphology of ACNFs by Scanning electron microscopy (SEM)

Fig. 21 (a to c) shows SEM images of ACNFs formed from 8 wt. % PAN solution with 1 wt. % Mn and pyrolysis at 800 ℃ (CN88-Mn1, Fig. 21a), ACNFs formed from 8 wt. % PAN solution with 1 wt. % Mn and pyrolysis at 900 ℃ (CN89-Mn1, Fig. 21b), ACNFs formed from 8 wt. % PAN solution with 1 wt. % Mn and pyrolysis at 1,000 ℃ (CN810-Mn1, Fig. 21c), respectively. Morphology of CN88-Mn1 with fiber deformation could be assume caused of nanofibers were solvent fused after deposited on the collector because of remaining solvent in the nanofibers and deformation by manganese agglomerate during burn-off at the surface due to the higher ratio of manganese on PAN fibers made carbon decomposition cause of after carbonization at 800 ℃ cannot make strong bond of carbon-based compared to CN89-Mn1, and CN810-Mn1 which less deformation of ACNFs. In addition, PAN nanofibers formed from 8 wt. % PAN solution with 1 wt.% Mn have a half smaller diameter than PAN nanofibers formed from 10 wt.% PAN solution with 1 wt.% Mn, can cause low thermal resistance.

Fig. 21 (d to g) shows SEM images of ACNFs formed from 10 wt.% PAN solution without manganese and pyrolysis at 900 ℃ (CN109, Fig. 21d), ACNFs formed from 10 wt.% PAN solution with 1 wt.% Mn and pyrolysis at 800 ℃ (CN108-Mn1, Fig. 21e), ACNFs formed from 10 wt.% PAN solution with 1 wt.% Mn and pyrolysis at 900 ℃ (CN109-Mn1, Fig. 21f), ACNFs formed from 10 wt.% PAN solution with 1 wt.% Mn and pyrolysis at 1,000 ℃ (CN1010-Mn1, Fig. 21g), respectively. Fig. 21d-g shows ACNFs with an average diameter ranging from 200 nm to 400 nm with smooth outer surface same as as-spun PAN nanofibers before treatment but cut in length according to cracking from thermal treating.

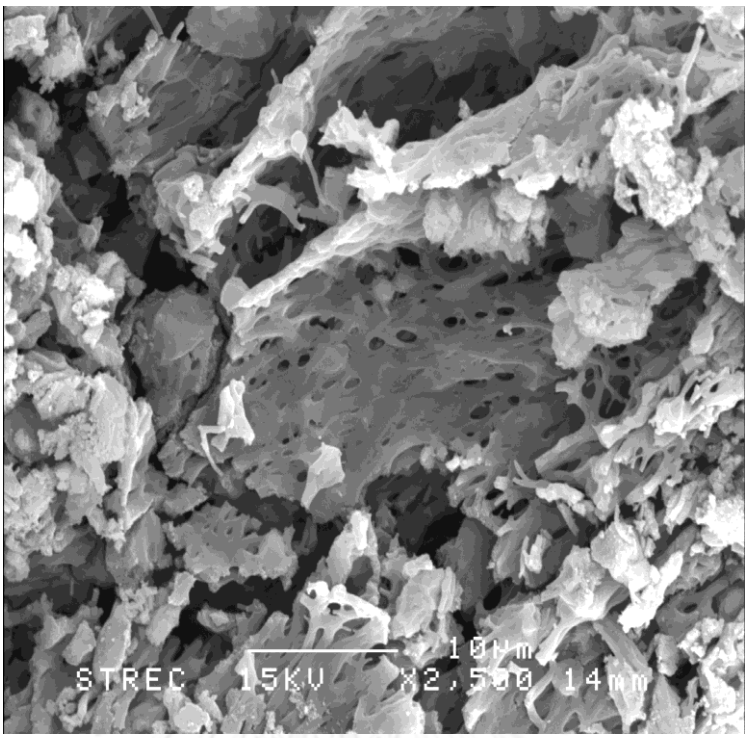

Fig. 21 (a) ACNFs formed from 8 wt. % PAN solution with 1 wt. % Mn and pyrolysis at 800 °C (CN88-Mn1)

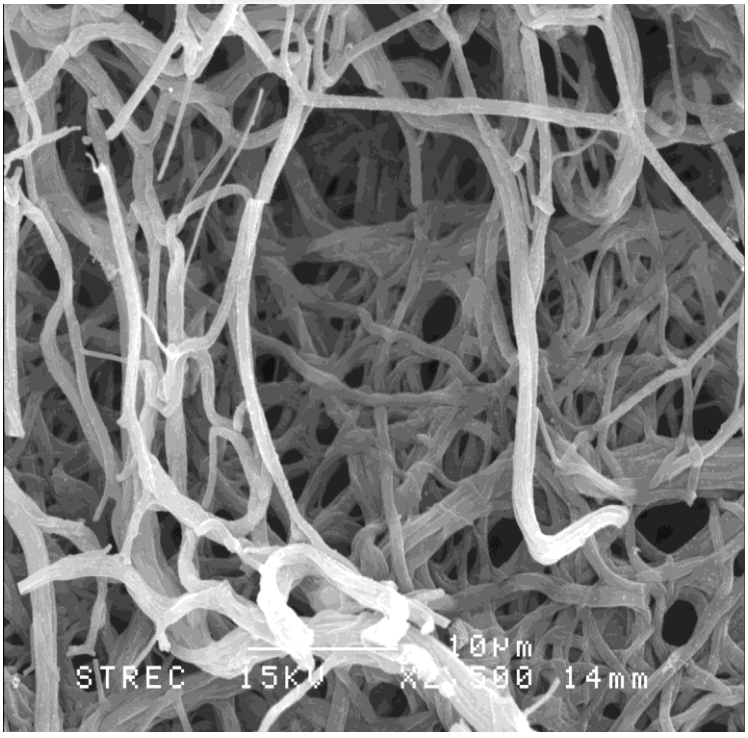

Fig. 21 (b) ACNFs formed from 8 wt. % PAN solution with 1 wt. % Mn and pyrolysis at 900 °C (CN89-Mn1)

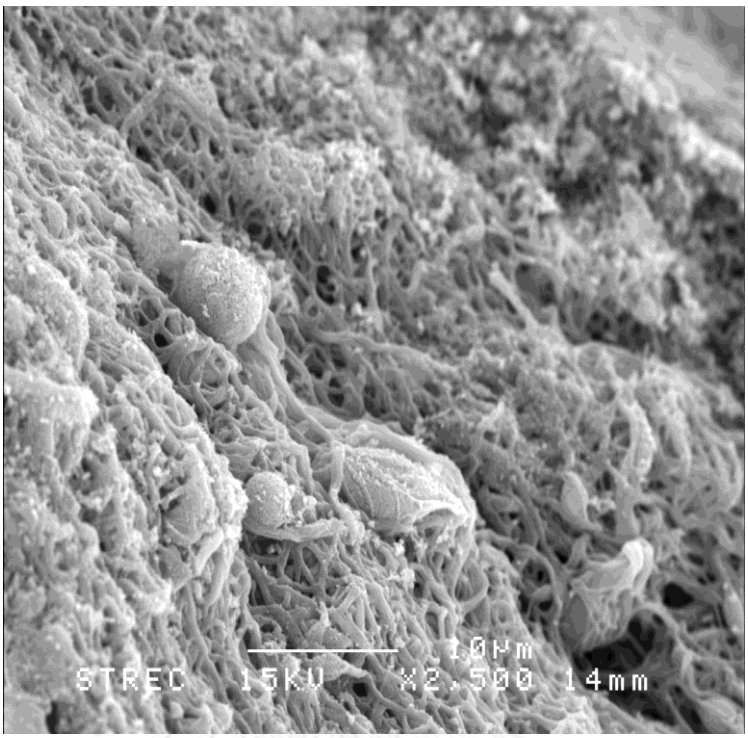

Fig. 21 (c) ACNFs formed from 8 wt. % PAN solution with 1 wt. % Mn and pyrolysis at 1,000 °C (CN810-Mn1)

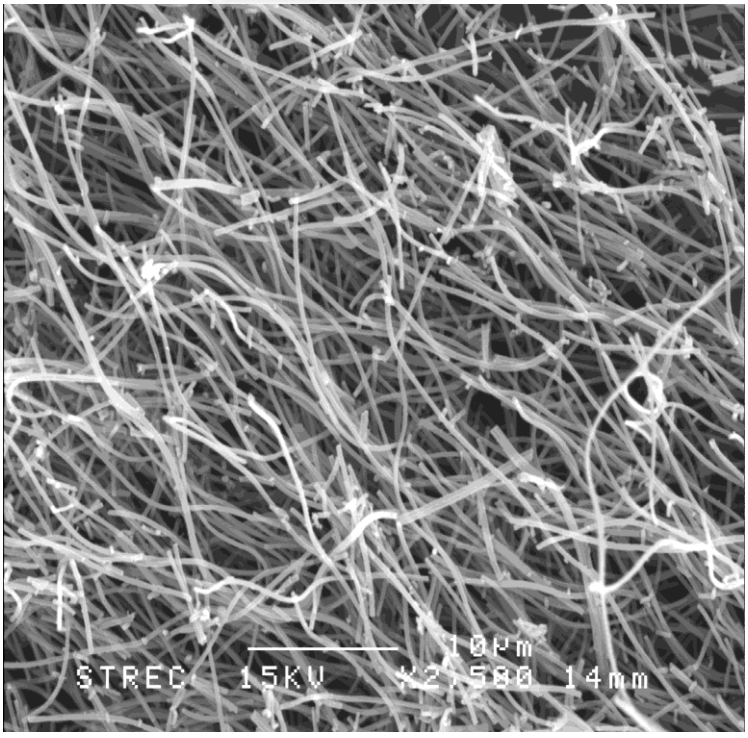

Fig. 21 (d) ACNFs formed from 10 wt. % PAN solution without Mn and pyrolysis at 900 °C (CN109)

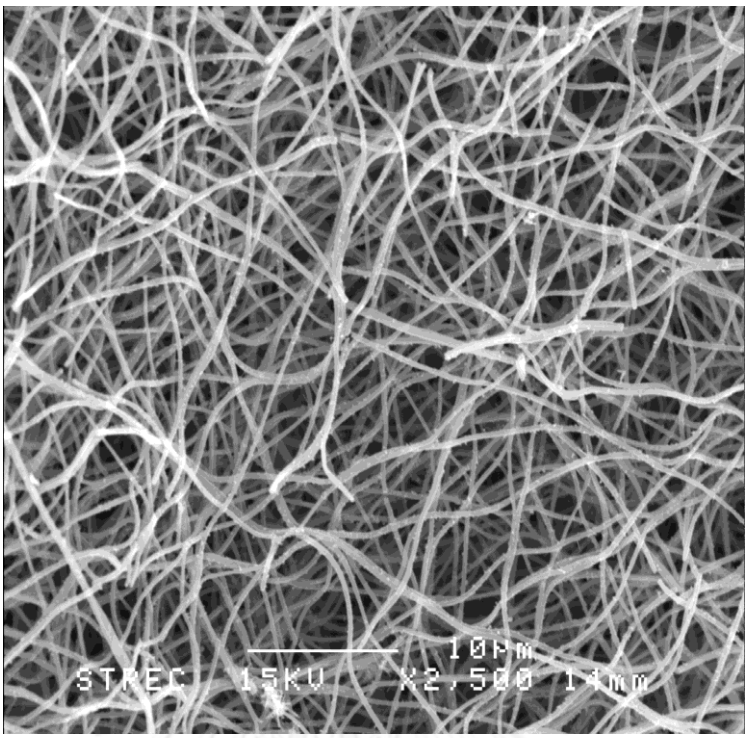

Fig. 21 (e) ACNFs formed from 10 wt. % PAN solution with 1 wt. % Mn and pyrolysis at 800 °C (CN108-Mn1)

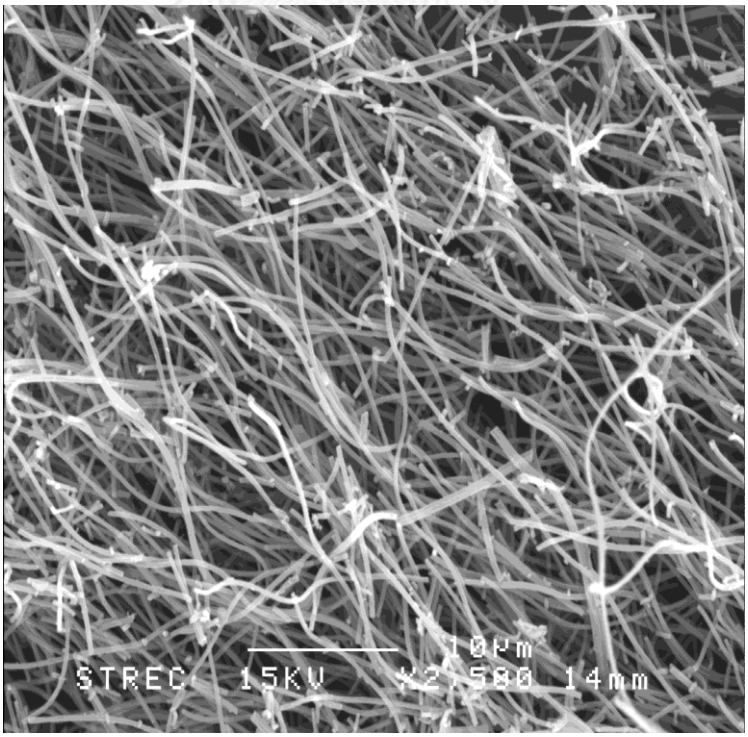

Fig 21 (f) ACNFs formed from 10 wt. % PAN solution with 1 wt. % Mn and pyrolysis at 900 °C (CN109-Mn1)

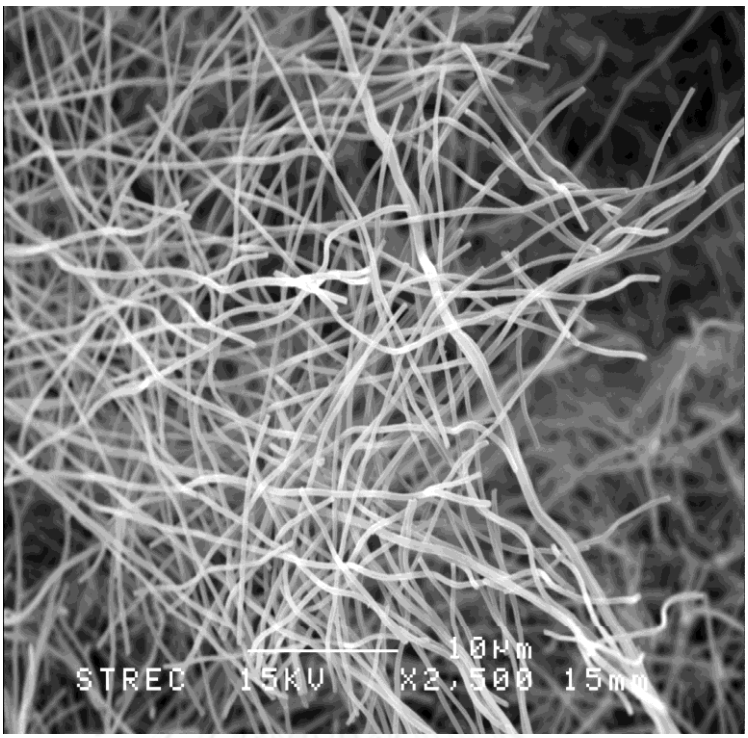

Fig. 21 (g) ACNFs formed from 10 wt. % PAN solution with 1 wt. % Mn and pyrolysis at 1,000 ℃ (CN1010-Mn1)

Table 4 shows the carbonization yield (yield of product after carbonization from as-spun PAN nanofibers calculated by percent remaining of product weight) and ACNFs yield (yield of product after activation from as-spun PAN nanofibers calculated by percent remaining of product weight). For CN88-Mn1 has a lowest yield since weak C-C bond in structure after carbonization at 800 ℃. Hence, higher PAN concentration with larger in fiber diameter can generate more ACNFs product cause of smaller diameter of fiber have low standing of thermal treatment. However, higher carbonization temperature increase will cause more product loss by burn-off.

Table 4 shows the carbonization yield and ACNFs yield of samples

Samples	Carbonization yields (% Based on as-spun PAN nanofibers)	ACNFs yields (% Based on as-spun PAN nanofibers)
CN88-Mn1	14%	2%
CN89-Mn1	27%	10%
CN810-Mn1	23%	10%
CN108-Mn1	58%	23%
CN109-Mn1	51%	16%
CN1010-Mn1	48%	15%

4.2.2 Functional group of ACNFs by Fourier transform infrared spectroscopy (FTIR)

Fig. 22 shows FTIR spectra of PAN nanofibers formed from 10 wt.% PAN with 1 wt. % Mn (Fig. 22a), stabilized 10 wt.% PAN with 1 wt.% Mn (Fig. 22b), pyrolyzed at 800 °C, 10 wt.% PAN with 1 wt.% Mn (Fig. 22c), CN108-Mn1 (Fig. 22d), and CN109 (Fig. 22e), respectively. The obtained FTIR spectra of PAN nanofibers reveal major peaks as shown in **Table 5**. After stabilization, the functional group of PAN nanofibers did not change but low intensity in 2243 cm^{-1} (Aliphatic nitrile) and 1252 cm^{-1} (Skeletal C-C vibration). This cause the nanofibers pick up oxygen molecules from the air and rearrange their atomic bonding pattern [18, 19]. After pyrolysis, there are low intensity in 3375 cm^{-1} (O-H stretch) and 2923 cm^{-1} (C-H stretch), however, at 1291 cm^{-1} (skeletal C-C vibration) has more board peak and intensity meanwhile at 2243 cm^{-1} (aliphatic nitrile) was disappears. This cause the nanofibers lose their non-carbon atoms, the remaining carbon atoms form tightly bonded carbon. After activation by steam, the peak at 3439 cm-1 (O-H stretch) has more board peak and intensity because of surface treatment by steam makes $-OH^{-}$ group on nanofibers surface. Then, functional groups of PAN nanofibers with Mn were changed to carbon-based materials which are suitable for VOCs adsorption but CN109 has functional group same as as-spun PAN nanofibers cause of has no Mn as chemically catalytic effect to reduce aliphatic nitrile.

Table 5 Functional groups detected by Fourier Transform Infrared Spectroscopy (FTIR) of PAN nanofibers with 1 wt. % Mn.

IR peaks	Wavelength (cm^{-1})					Assignment
	10% PAN	Stabilized	Pyrolyzed	CN108-Mn1	CN109	
1	3455	3443	3375	3439	3450	O-H stretch
2	2938	2924	2923	2924	2925	C-H stretch
3	2243	2243	-	-	2244	Aliphatic nitrile
4	1626	1626	-	1620	1631	Carbonyl
5	-	-	1578	-	-	C-C stretch
6	1453	1453	-	-	1454	C-N stretch
7	1358	1370	-	-	1360	C-N stretch
8	1252	1252	1291	1268	1253	Skeletal C-C vibration
9	1073	1072	-	-	1074	C-O stretch

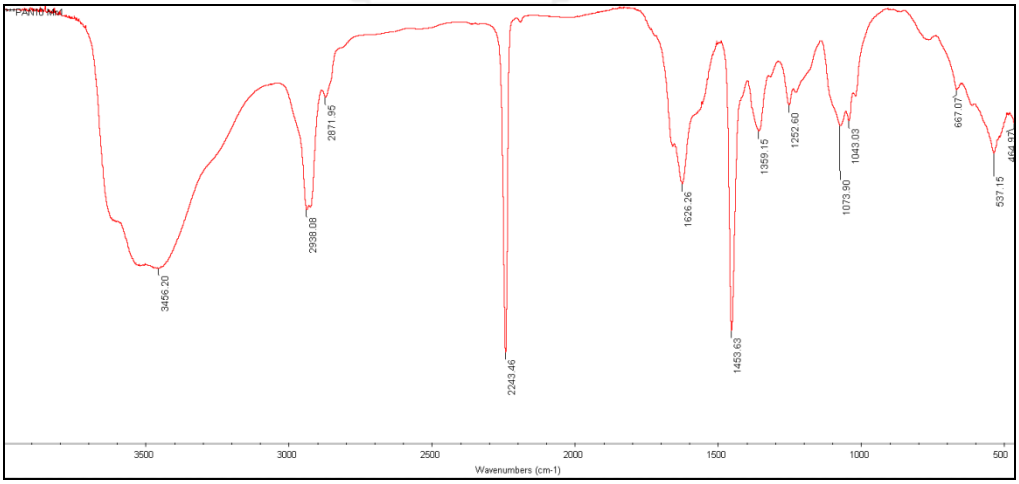

Fig. 22 (a) shows FTIR spectra of 10 wt. % PAN with 1 wt. % Mn

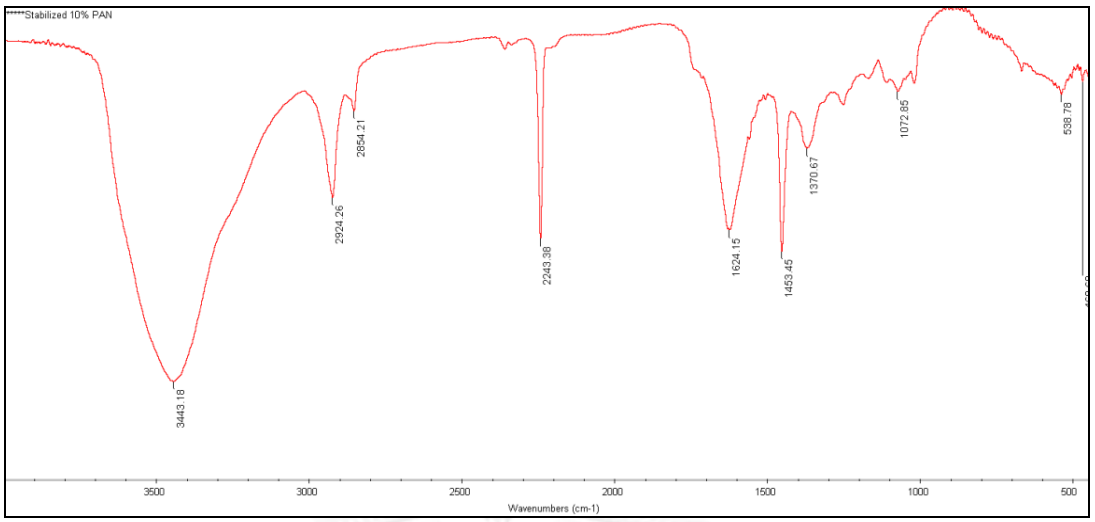

Fig. 22 (b) shows FTIR spectra of Stabilized 10 wt. % PAN with 1 wt. % Mn

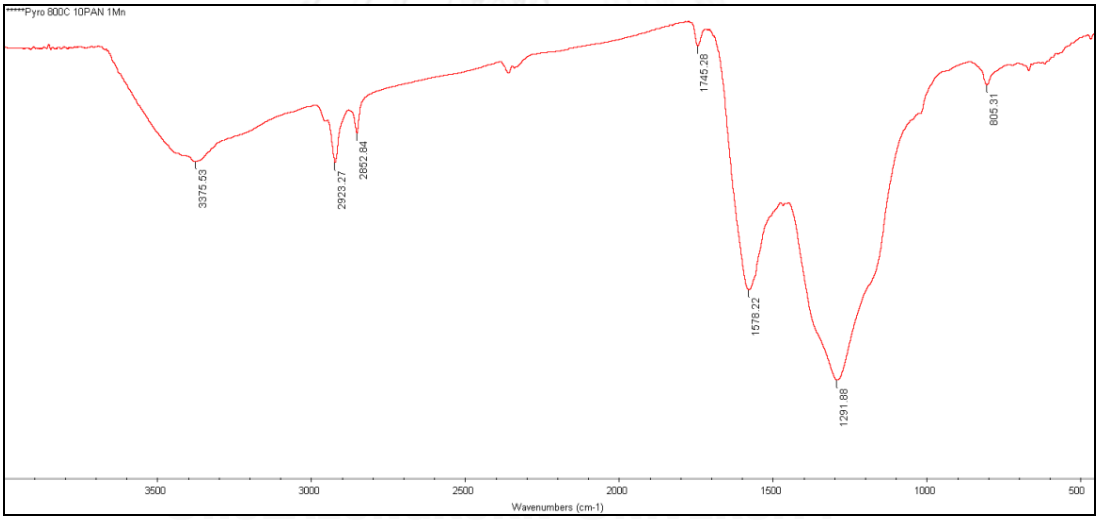

Fig. 22 (c) shows FTIR spectra of Pyrolysis at 800 ℃ 10 wt. % PAN with 1 wt. % Mn

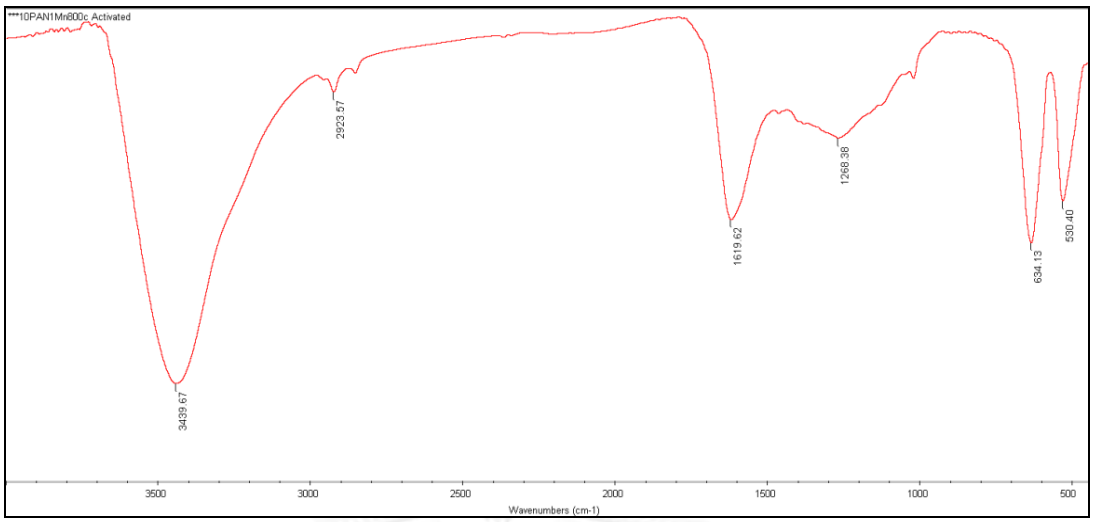

Fig. 22 (d) shows FTIR spectra of CN108-Mn1

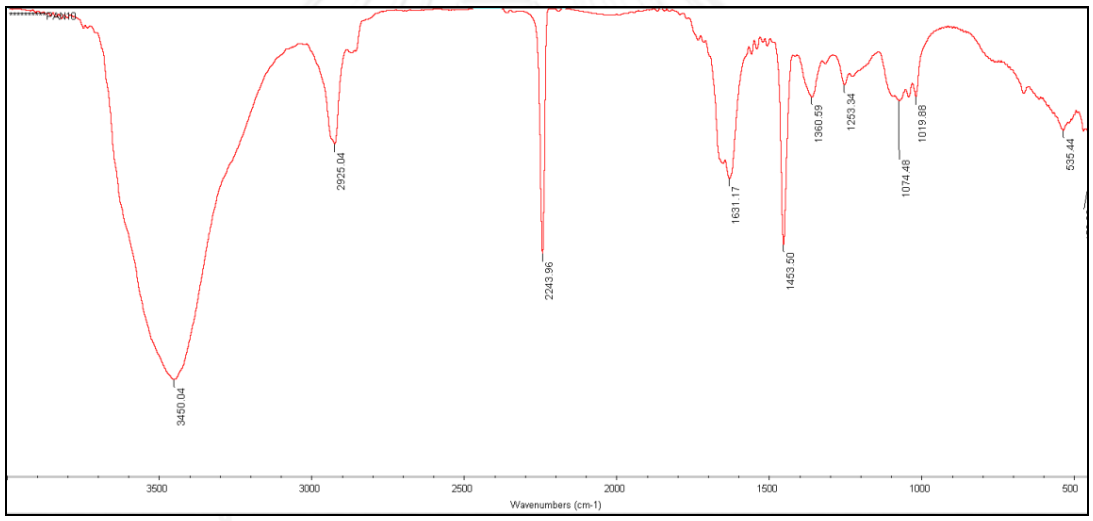

Fig. 22 (e) shows FTIR spectra of CN109

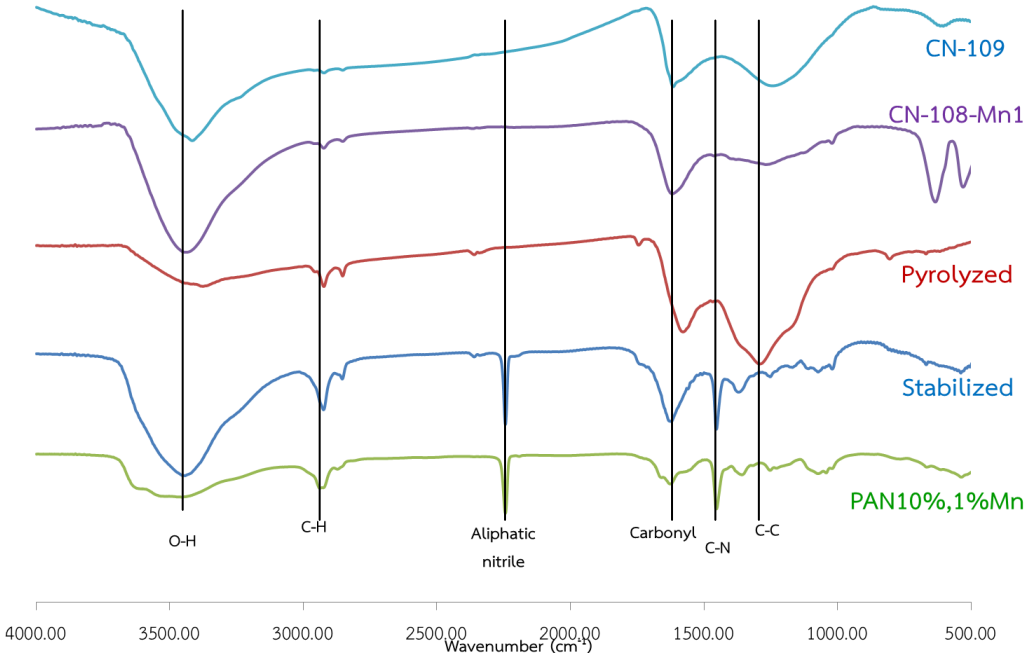

Fig. 22 (f) shows FTIR spectra compare functional group of each sample step

4.2.3 Pore Characteristics of the samples by Automatic specific surface area/pore size distribution measurement

The embedding Mn particles in carbon nanofibers aim to control the pore characteristics, such as the specific surface area and micropore volume using the optimal activation condition. The pore channels are formed by the following two behaviors [3, 48]. The former results in the formation of pore channels by the migration of metal particles during burn-off and the latter cause the creation of pores by accelerating the activating rate by the metal particles during burn-off. In other words, the metal particles migrate easily through the carbon fiber because of faster decomposition of carbon next to manganese by chemically catalytic effect, compared to carbon without manganese.

Table 6 shows the pore characteristics, such as the specific surface area by BET equation, total pore volume and micropore volume by *t*-plot and mean pore diameter by BET equation according to MN loading on ACNFs.

The pore characteristics of were not enhanced by embedding 1 wt.% Mn, specific surface area of CN109 was larger than other embedded-manganese ACNFs but still lower than other previously synthesis by many researchers, due to the

activation condition not suitable for manganese to improve specific surface area compare to commercial activated carbon. In addition, low density of steam boiled at 100 °C in activation process could not treat surface of ACNFs to enhance specific surface area because of low pressure of steam cannot react with carbon to create micropore inside ACNFs. In other words, activation process may be occurring at outer surface of ACNFs. Hence, Specific surface area and total pore volume as shown in **Table 6** are natural porous of ACNFs or from surface treatment of low density steam.

Table 6 Pore characteristics of the samples

Samples	Mn[a] loading (%)	S.S.A.[b] (m^2/g)	T.P.V.[c] (cm^3/g)	M.P.V.[d] (cm^3/g)	M.P.D.[e] (nm)	A.C.[g] (toluene g /sample 100 g)
CN88-Mn1	16.4	359	0.269	0.240	3.00	11.1
CN89-Mn1	2.1	238	0.157	0.158	2.60	9.0
CN810-Mn1	4.5	343	0.260	0.240	3.03	15.6
CN108-Mn1	0.9	368	0.320	0.260	3.47	25.8
CN109-Mn1	0.4	435	0.435	0.289	4.00	17.8
CN1010-Mn1	0.4	485	0.709	0.356	5.84	26.8
CN109	0	517	0.400	0.371	3.10	26.4
Activated C[g]	0	593	0.397	0.383	2.68	20.0

[a] This data were obtain from SEM-EDS analysis.

[b] Specific surface area by BET.

[c] Total pore volume.

[d] Micropore volume by *t*-plot.

[e] Mean pore diameter

[f] Adsorption capacity.

[g] Commercial grade activated carbon

Fig. 23 shows the adsorption isotherms of N_2 at 77 K of CN109, CN108-Mn1, CN109-Mn1, CN1010-Mn1. CN88-Mn1, CN89-Mn1, CN810-Mn1, and commercial activated carbon. The patterns of all isotherms represent micropore adsorption as the typical type I, except for CN1010-Mn1 shown pattern seem as monolayer coverage is followed by multilayering at high relative pressures acts as mixed micro- and meso-porosity produce Type II isotherms.

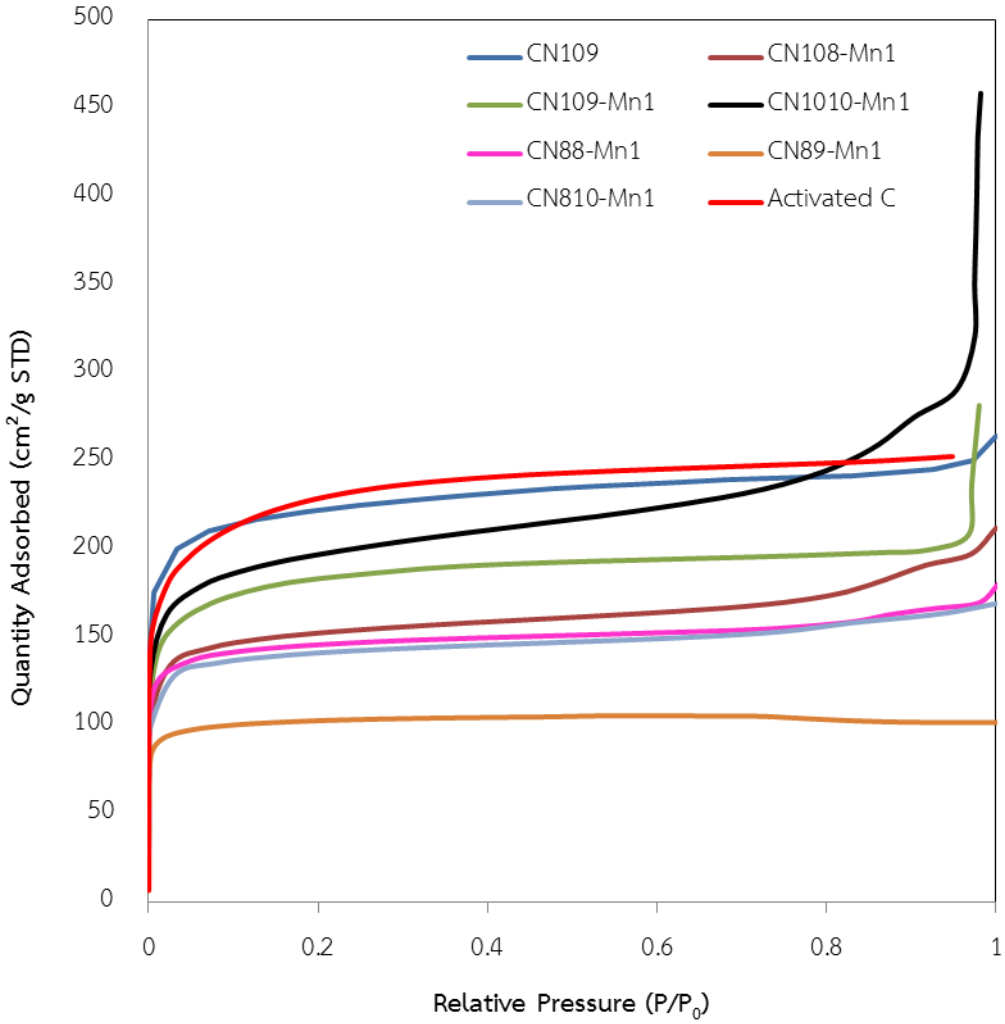

Fig. 23 Nitrogen adsorption isotherm (77 K) of samples.

Fig. 24 shows pore size distribution by BJH-plot. The peaks reveal most of samples are in micropore except CN109-Mn1 and CN1010-Mn1 can notice mesopore was forming. The propose for mesopore forming could assume that low pressure steam could react only outer surface of carbon nanofibers then when micropore on outer surface was forming, the remaining steam continue react with available micropore expand to mesopore while manganese particles migration to outer surface of ACNFs cold react with steam and interrupt forming micropore too.

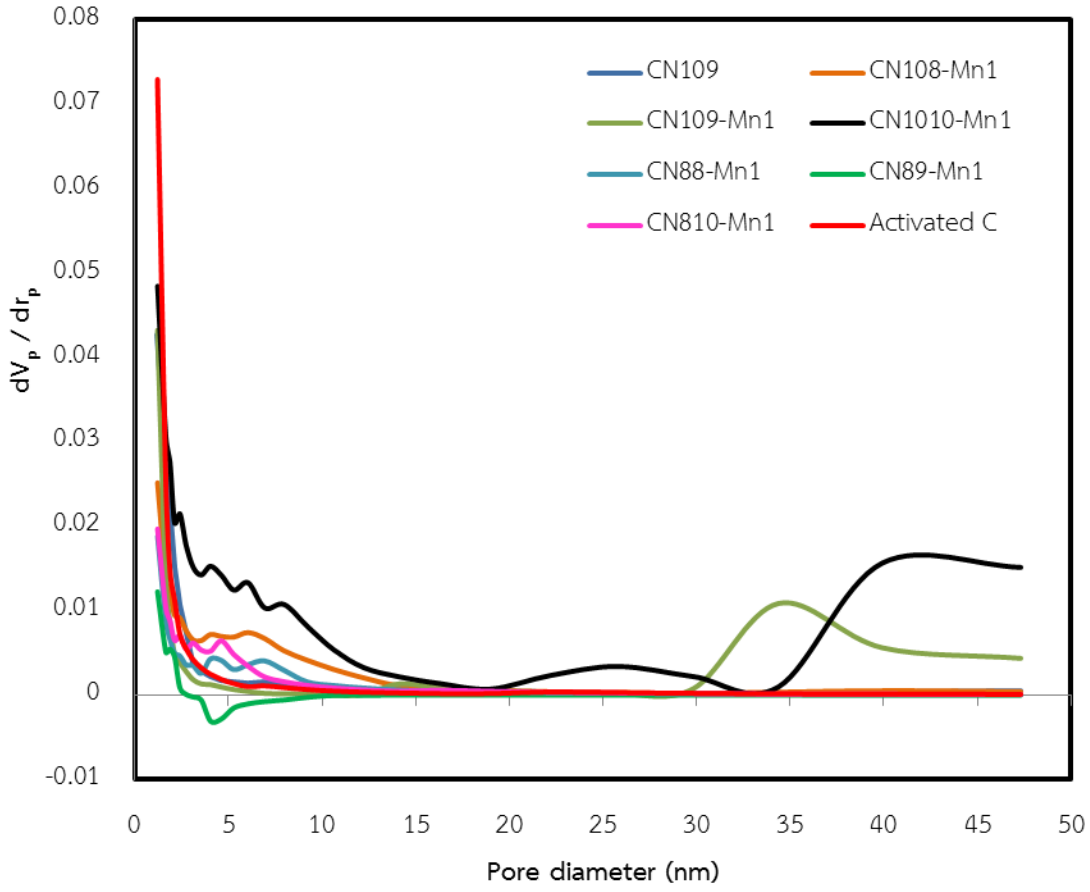

Fig. 24 Pore size distribution by BJH-plot

Fig. 25 shows micropore size distribution by MP plot. The peak micropore sizes of all samples are about 0.6 nm in range of micropore could adsorb toluene of approximately 3.7 Å (width) x 7.0 Å (length). For CN1010-Mn1 has low distribution compared to other samples. Meanwhile, commercial activated carbon has large pore size distribution from uncontrolled size of activated carbon in the process. The synthesized ACNFs have micropore size distribution in the same pattern because of uniform size of nanofibers diameter.

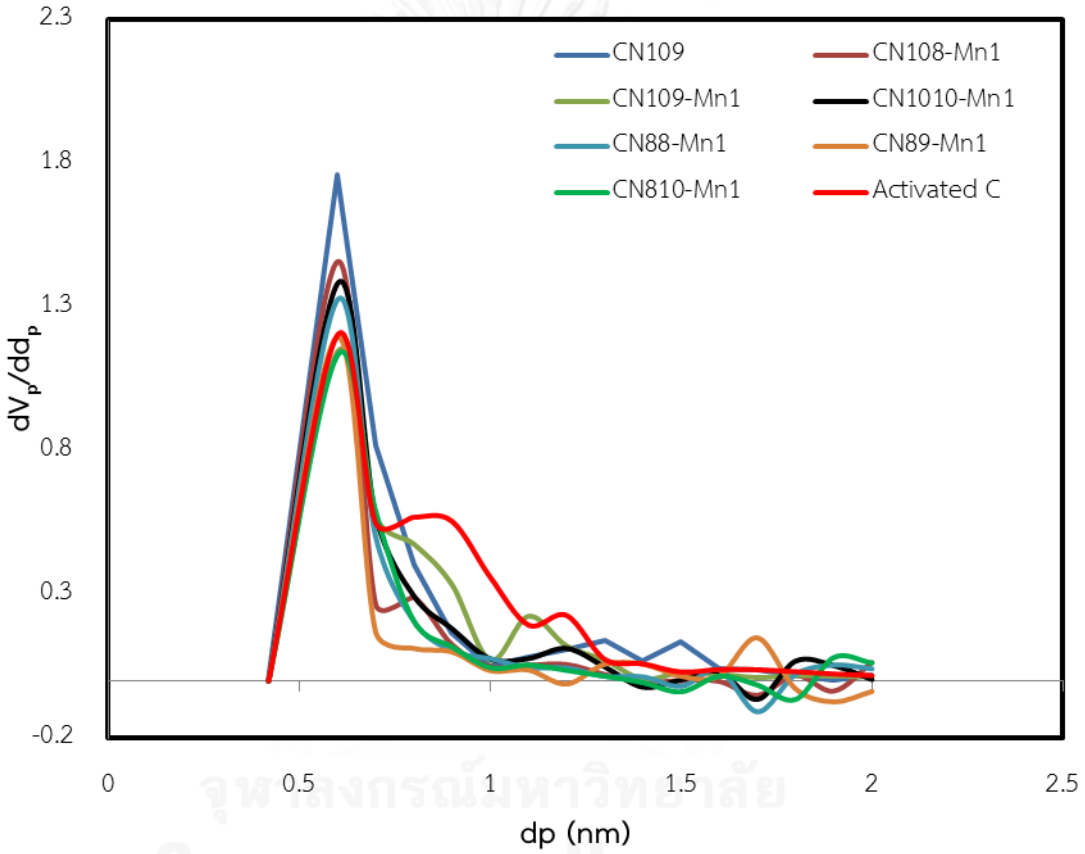

Fig. 25 Micropore size distribution by MP plot

4.2.4 Element surface composition determined from SEM-EDS

Table 7 shows the manganese loading on the carbon fibers and oxygen to carbon ratio obtained from SEM-EDS. Percentage of oxygen content in ACNFs were too high compared to previous research due to inappropriate activation condition make ACNFs adsorbed more moisture in ACNFs. Then, surface treatments of ACNFs that have high oxygen to carbon ratio (O/C ratio) represent more polarity of the ACNFs surface may not suitable for toluene adsorption.

For CN-88-Mn1 has highest manganese content as 16.41% due to the rest of carbon content has drop down in process of carbonization and activation. Since the rest of carbon content has drop down in process of carbonization followed by activation, manganese content has increase more than 1 wt. % from precursor and CN88-Mn1 has highest manganese content cause of highest loss of carbon due to weak C-C bond in structure.

Table 7 Quantitative analysis of elemental composition determined from SEM-EDS

Samples	Total carbon (%)	Total oxygen (%)	Total manganese (%)	O/C ratio
CN88-Mn1	34.25	49.35	16.41	1.441
CN89-Mn1	81.64	16.31	2.05	0.200
CN810-Mn1	77.25	18.29	4.46	0.237
CN108-Mn1	72.41	26.74	0.86	0.369
CN109-Mn1	72.07	27.53	0.40	0.382
CN1010-Mn1	75.38	24.17	0.45	0.321
CN109	83.06	16.94	0	0.204

4.3 Toluene adsorption

Fig. 26 and **Table 6** show breakthrough curves and adsorption capacity obtained from toluene adsorption at a toluene concentration about 150 to 160 mg/L at 30 °C. The concentrations of inlet and outlet toluene vapor for each batch were measured by gas chromatography. The toluene capacity calculated from each inlet and outlet batch value.

CN1010-Mn1 showed the highest toluene adsorption capacity was 26.83 g toluene/100 g adsorbent due to the highest total pore volume (T.P.V. 0.709 cm^3/g) and larger mean pore diameter (5.84 nm) but lower capacity when compare to other research caused of lower specific surface area 485 m^2/g and high O/C ratio (0.321). Meanwhile, activated carbon which highest specific surface area (593 m^2/g) can adsorb 20.0 g toluene/100 g adsorbent due to low total pore volume (0.397 cm^3/g) compared to CN1010-Mn1.

For CN109 has specific surface area is 517 m^2/g, total pore volume is 0.400 cm^3/g could adsorb toluene 26.83 g toluene/100 g adsorbent compare with CN109-Mn1 has specific surface area is 435 m^2/g, total pore volume is 0.435 cm^3/g could adsorb toluene 17.8 g toluene/100 g adsorbent. The specific surface area of CN109-Mn1 was reduced because the Mn particles were agglomerated on the surface cause of the remaining of Mn in ACNFs was too high due to inappropriate activated condition.

Fig. 27 shows relativity of specific surface area (S.S.A.) and toluene adsorption capacity for each adsorbent. The toluene adsorption capacity has relative to S.S.A., T.P.V. and O/C ratio.

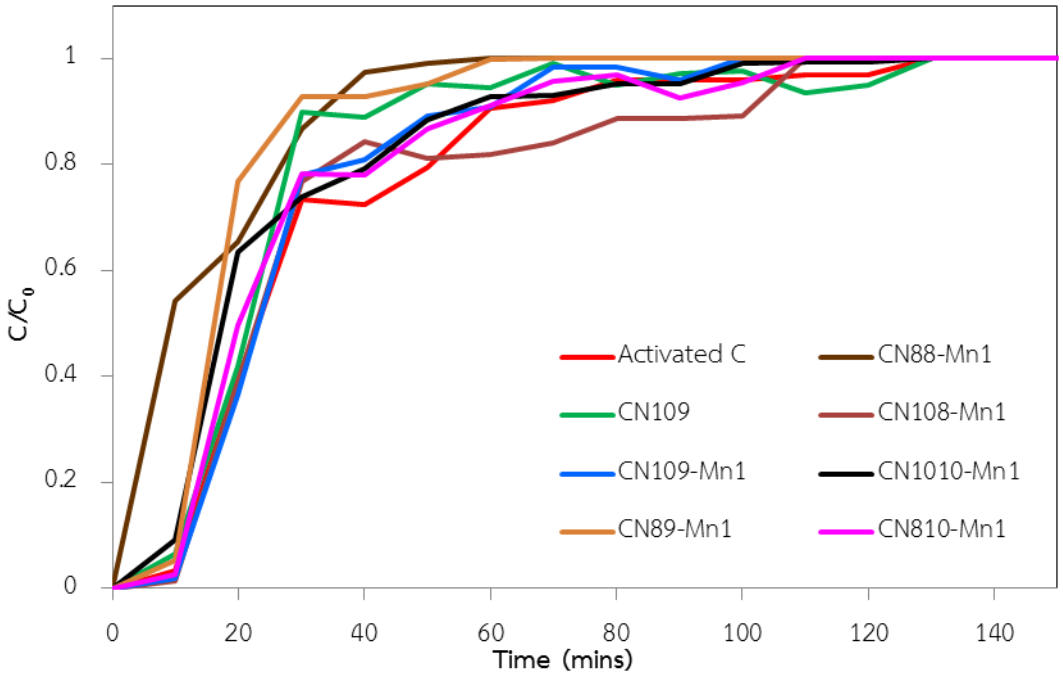

Fig. 26 Breakthrough curves of toluene adsorption

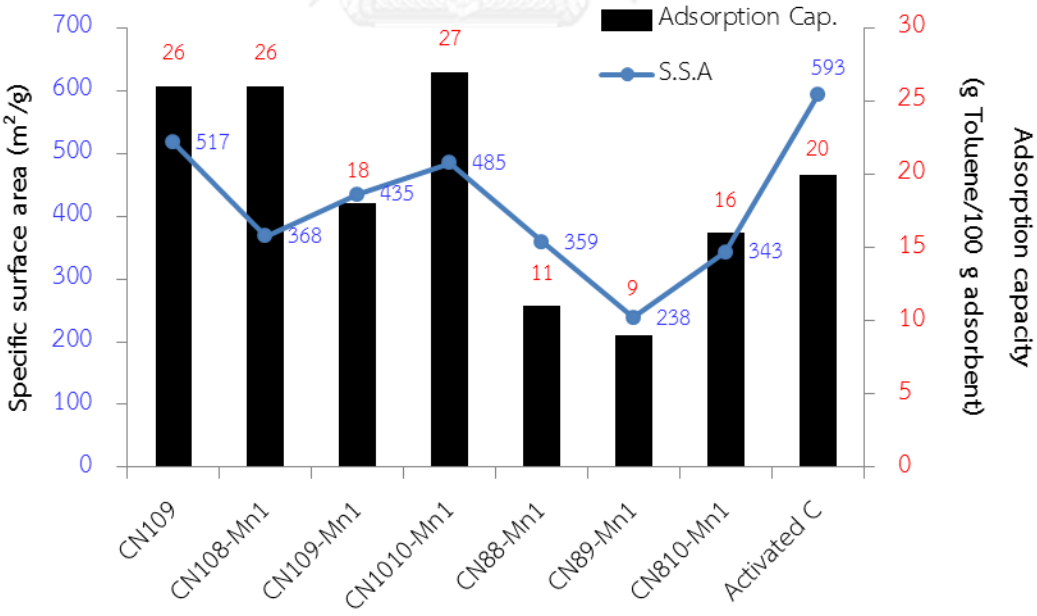

Fig. 27 shows relativity of specific surface area and toluene adsorption capacity

4.4 The weight loss of toluene on ACNFs after adsorbed was estimated by Thermogravimetric analysis.

Fig. 28 show TGA profiles of sample after were adsorbed toluene vapor. Toluene vapor on ACNFs could remove by heating up to 400 ℃ to investigate weight loss cause of toluene, its mean toluene were adsorbed by physical adsorption as well as N_2 adsorption. The amounts of burn-off of toluene begin at 50 ℃ to near 400 ℃ because of toluene has adsorbed and penetrate to inside the micropore in samples. The percentage of weight loss could relate to toluene adsorption capacity show in **Table 8**.

Table 8 The percentage of weight loss from TGA and toluene adsorption capacity

Samples	A.C.[g] (toluene g /sample 100 g)	Weight loss (%)
CN88-Mn1	11.1	19.9
CN89-Mn1	9.0	16.5
CN810-Mn1	15.6	21.3
CN108-Mn1	25.8	23.0
CN109-Mn1	17.8	18.7
CN1010-Mn1	26.8	20.4
CN109	26.4	23.1
Activated C [g]	20.0	22.8

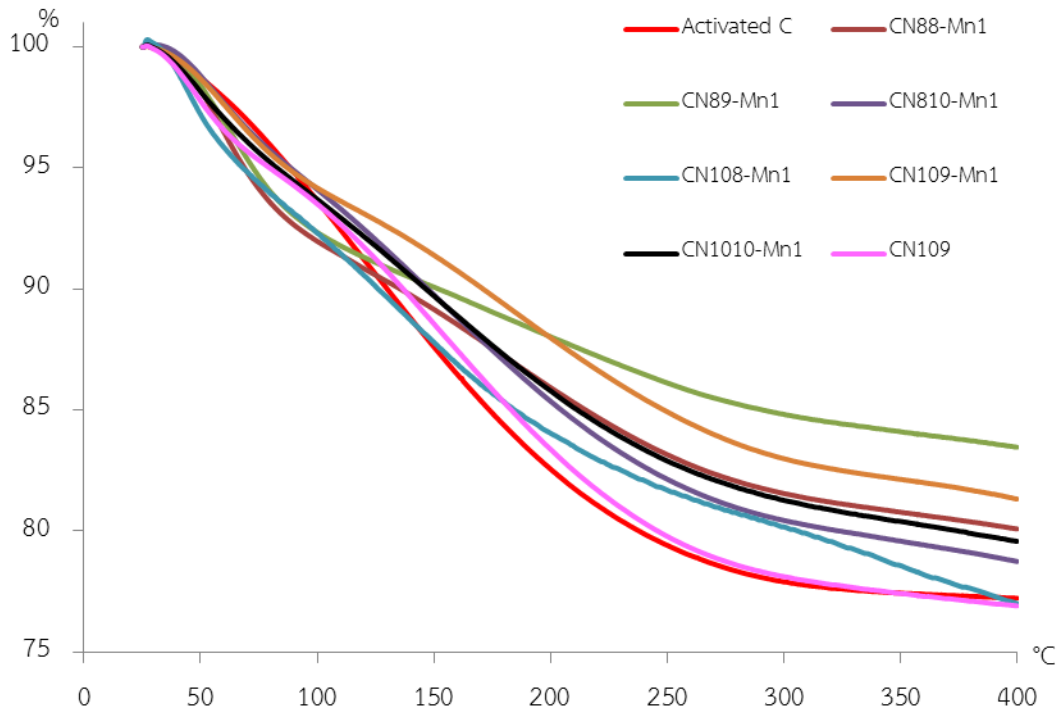

Fig. 28 TGA profiles of samples after adsorbed toluene

Fig. 29 (a to h) show the functional groups of samples before toluene adsorption, after adsorption and after TGA test. The functional groups of samples maintain the same as original because no chemical bonds are formed during physical adsorption and all samples could regenerate by heat without change in structure.

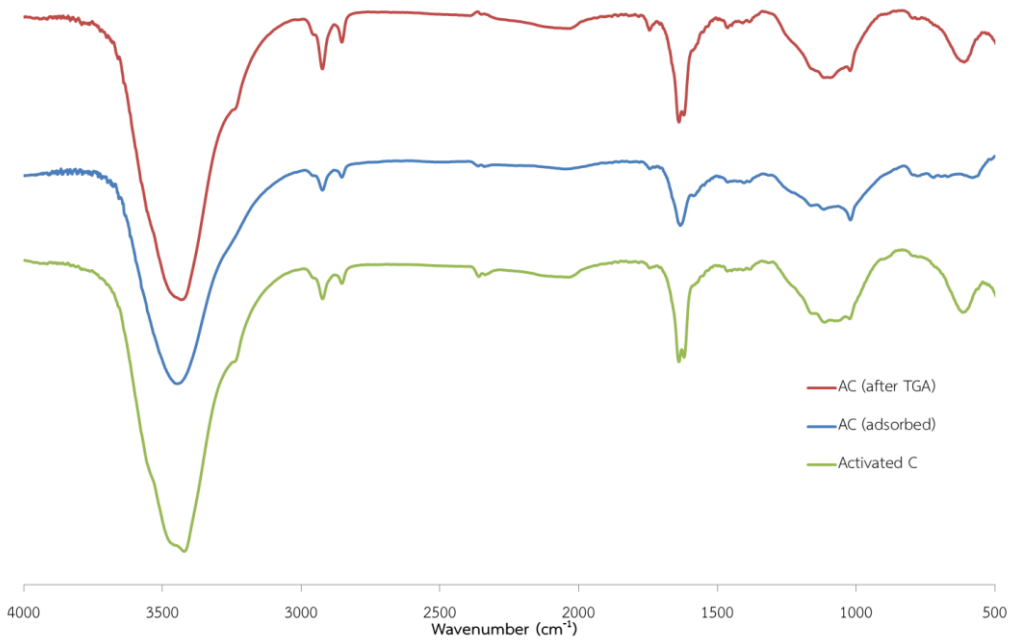

Fig. 29 (a) FTIR spectra of commercial activated carbon

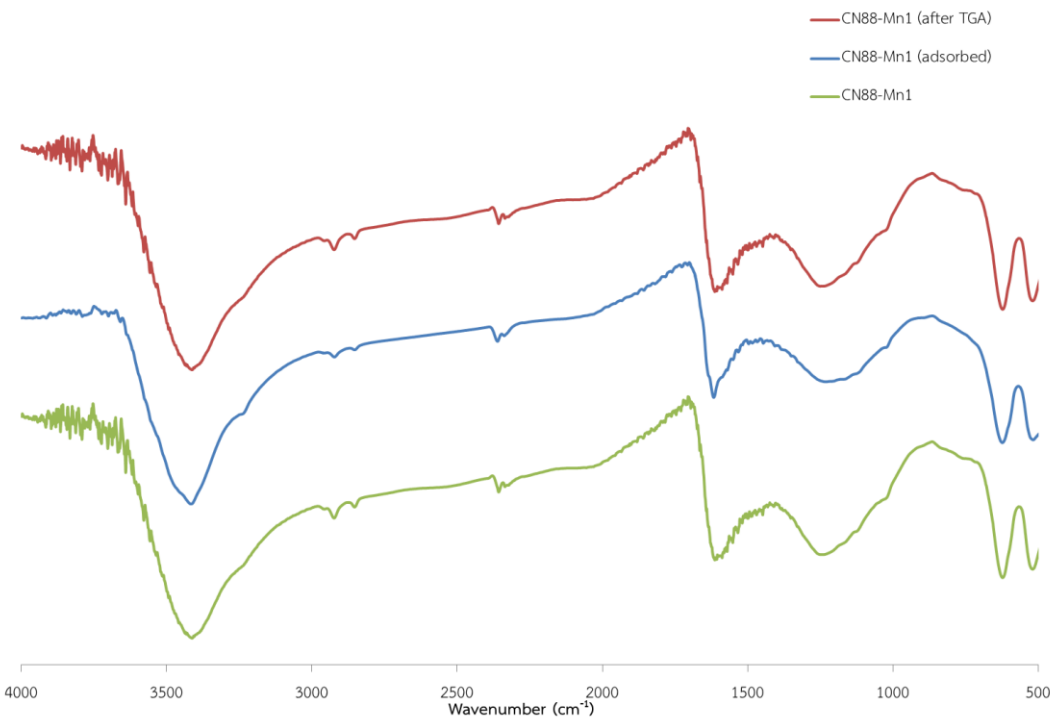

Fig. 29 (b) FTIR spectra of CN88-Mn1

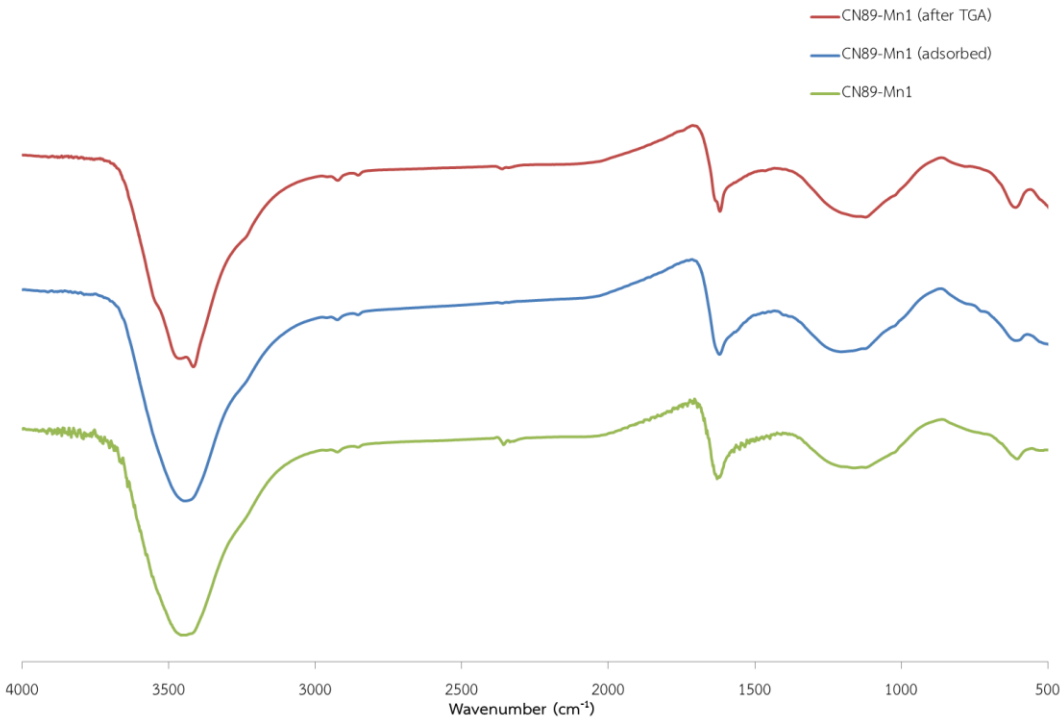

Fig. 29 (c) FTIR spectra of CN89-Mn1

Fig. 29 (d) FTIR spectra of CN810-Mn1

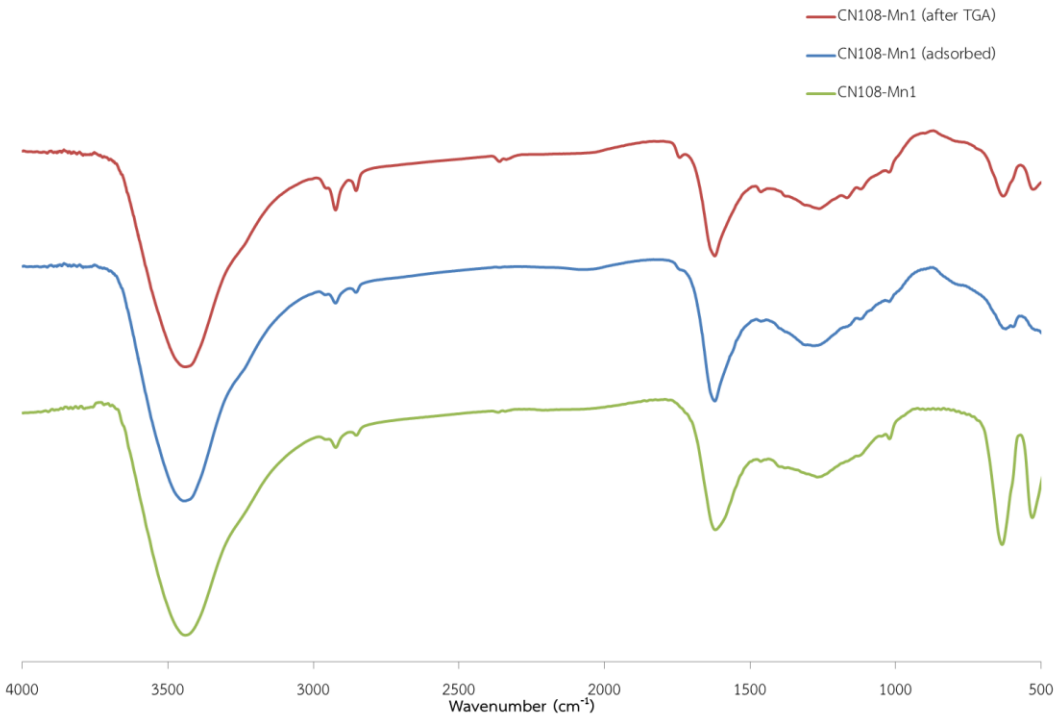

Fig. 29 (e) FTIR spectra of CN108-Mn1

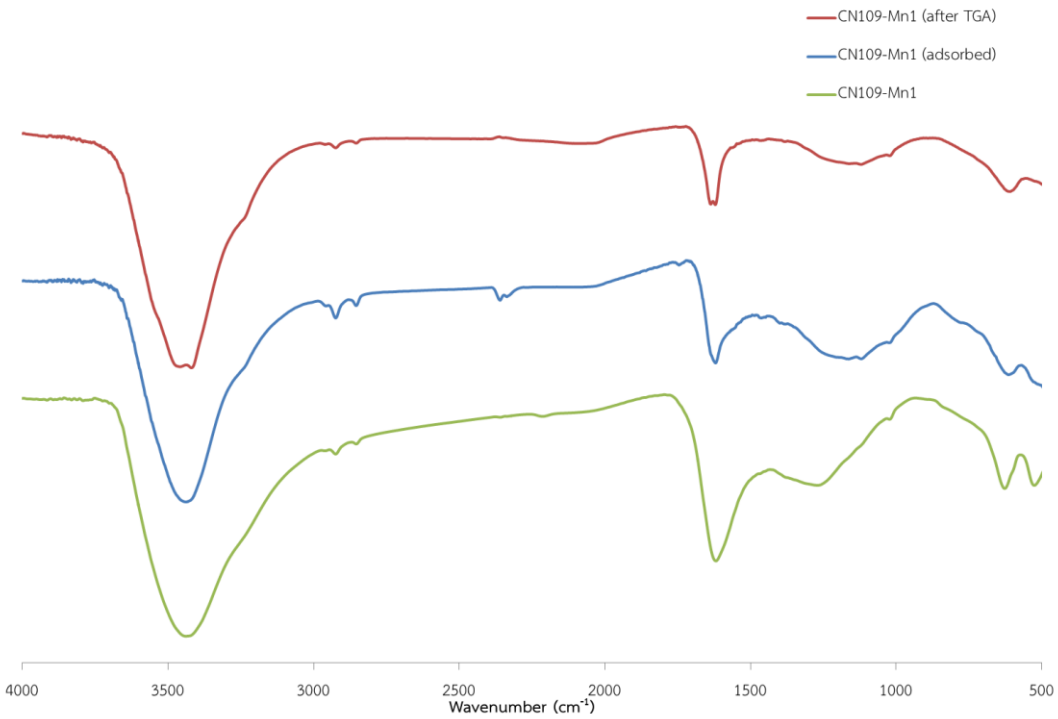

Fig. 29 (f) FTIR spectra of CN109-Mn1

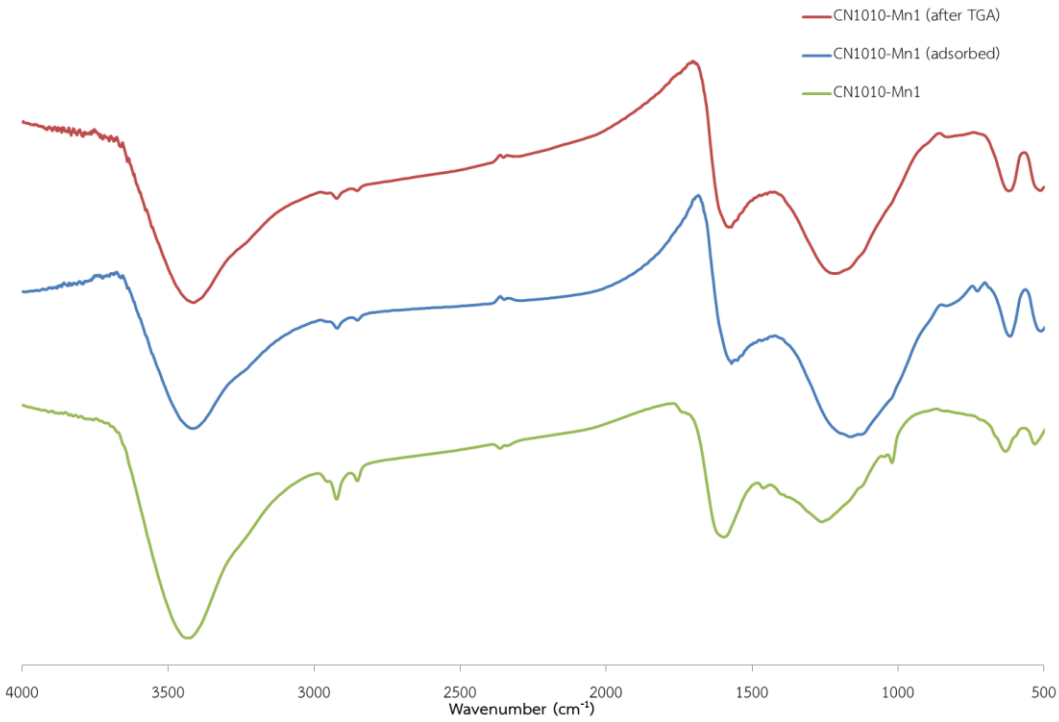

Fig. 29 (g) FTIR spectra of CN1010-Mn1

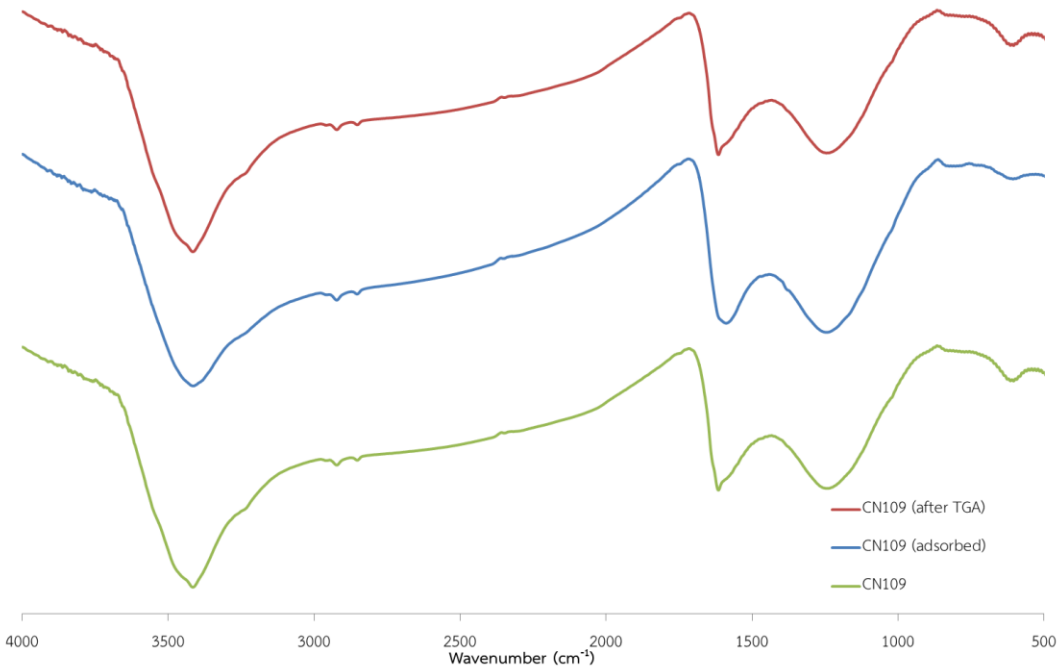

Fig. 29 (h) FTIR spectra of CN109

The propose mechanism of toluene adsorption is physical adsorption. The adsorption capacity of toluene depends on T.P.V., M.P.D., O/C ratio, S.S.A. and mesopore volume, respectivity.

CHAPTER 5
CONCLUSION AND RECOMMENDATION

5.1 Conclusion

The concentrations of PAN in DMF for this study are 8% and 10%. The average diameters of the PAN fibers were in the range of 200 to 500 nm. After stabilization, carbonization, and activation, the functional groups of PAN nanofibers were changed to that of carbon-based materials which are suitable for VOCs adsorption. The activation yields of ACNFs depend on the pyrolysis temperature. The higher the temperature is, the more products were lost during the pyrolysis but enhance the specific surface area after activated due to stronger C-C bond. The results of pore characteristics show that ACNFs prepared from the solution with high PAN content (i.e. 10% PAN) have higher specific surface area and larger micropore volume than that prepare from lower PAN content (i.e., 8% PAN), although other conditions such as fiber density, crystalline structure and amorphous carbon structure were found to be the same. The ACNF carbonized at 1,000 °C showed the highest toluene adsorption capacity of 26.83 g toluene/100 g adsorbent due to the highest total pore volume and large mean pore diameter. However, when compared to other research the specific surface area was still lower while having high O/C ratio. Moreover, manganese did not enhance toluene adsorption capacity because low steam density and pressure used in the activation was low and remaining manganese in ACNFs become agglomerated on surface and interrupt activation process.

5.2 Recommendation for future work

5.2.1 In the activation process have use high-temperature steam to increase the concentration and vapor pressure of water vapor for improve higher porosity. The optimal activation condition maybe enhance pore characteristic especially S.S.A., micropore volume and O/C ratio.

5.2.2 In order to control the concentration of outlet toluene should be use toluene gas better to use liquid.

5.2.3 Should be analyze manganese content of ACNFs after calcination and after activation for investigate changing of manganese in the sample.

5.2.4 The application of ACNFs for toluene adsorption, if fixed volume of adsorption bed while ACNFs could pack with low packing density compared to granule activated carbon. But ACNFs in form of fiber mats could adsorb toluene higher than granule activated carbon in term of gram of toluene on gram of adsorbent. In practical, to improve toluene adsorption capacity should pack ACNFs in bed with packing density nearly or equal to granule activated carbon. In the other word, if need to adsorb fixed volume of toluene could use less amount of ACNFs instead of granule activated carbon in packed bed.

5.2.5 All of experiment results should be repeated to confirm the obtained results.

REFERENCES

[1] http://www.npc-se.co.th.

[2] http://www.thaigoodview.com/node/46599).

[3] G Y Oh, Y W Ju, H R Jung, and W J Lee, "Preparation of the novel manganese-embedded PAN-based activated carbon nanofibers by electrospinning and their toluene adsorption," Journal of Analytical and Applied Pyrolysis, vol 81, pp 211-217, Mar 2008.

[4] Textile World Nano Technology and Nonwoven, P 52, November 2003.

[5] Bhat Gajanan and Lee Youneung, Recent advancements in Electrospun nanofibers, Proceedings of the twelfth international symposium of Processing and Fabrication of Advanced materials, Ed TS Srivatsan & RA Vain, TMS, 2003.

[6] http://wwwnanospidercz/nanofibersphp.

[7] นพภาพร พานิช และคณะ "ตำราระบบบำบัดมลพิษอากาศ" จัดทำโดย กรมโรงงานอุตสาหกรรม ร่วมกับศูนย์บริการวิชาการแห่งจุฬาลงกรณ์มหาวิทยาลัย, มีนาคม 2547.

[8] Electrostatic spinning of Nanofibers spin Technologies, Chattanooga, TN.

[9] M Jahangiri, S J Shahtaheri, J Adl, A Rashidi, H Kakooei, A R Forushani, M R Ganjali, and A Ghorbanali, "The Adsorption of Benzene, Toluene and Xylene (BTX) on the Carbon Nanostructures: The Study of Difference Parameters," Fresenius Environmental Bulletin, vol 20, pp 1036-1045, 2011.

[10] H Katepalli, M Bikshapathi, C S Sharma, N Verma, and A Sharma, "Synthesis of hierarchical fabrics by electrospinning of PAN nanofibers on activated carbon microfibers for environmental remediation applications," Chemical Engineering Journal, vol 171, pp 1194-1200, Jul 2011.

[11] G Y Oh, Y W Ju, M Y Kim, H R Jung, H J Kim, and W J Lee, "Adsorption of toluene on carbon nanofibers prepared by electrospinning," Science of the Total Environment, vol 393, pp 341-347, Apr 2008.

[12] http://wwwdesigninsitedk/htmsider/m0981htm.

[13] G I,Taylor, Proc Roy Soc London, A313, 453 (1969).

[14] L Wannatong, A Sirivat, P Supaphol, Polymer International 2004, 53, 1851.

[15] M M Demir, I Yilgor, E Yilgor, B Erman, Electrospinning of polyurethane fibers, Polymer 2002; 43:3303–9.

[16] HQ Liu, YL Hsieh, Ultrafine fibrous cellulose membranes from electrospinning of cellulose acetate J of Polymer Science Part B: Polymer Physics 2002; 40:2119–29.

[17] H Fong, DH Reneker, Elastomeric nanofibers of styrene-butadiene-styrene triblockcopolymer J Polymer Science: Part B Polymer Physics 1999; 37(24):3488–93.

[18] JM Deitzel, J Kleinmeyer, D Harris, NCB Tan, The effect of processing variables on the morphology of electrospun nanofibers and textiles Polymer 2001; 42:261–72.

[19] SK Nataraj, KS Yang, TM Aminabhavi, Polyacrylonitrile-based nanofibers—A state-of-the-art review, Progress in Polymer Science, Volume 37, Issue 3, March 2012, Pages 487-513.

[20] A Suthat, G Chase, Chemical Engineer 2001:26–8.

[21] D Groitzsch, E Fahrbach, US patent 4,618,524, 1986.

[22] HL Schreuder-Gibson, P Gibson, K Senecal, M Sennett, J Walker, W Yeomans, et al, Protective textile materials based on electrospun nanofibers Journal of Advanced Materials 2002; 34(3): 44–55.

[23] JM Deitzel, J Kleinmeyer, D Harris, NCB Tan, The effect of processing variables on the morphology of electrospun nanofibers and textiles, Polymer 2001; 42:261–72.

[24] http://wwwmtecorth/indexphp/2013-05-29-09-06-21/2013-05-29-09-39-49/512.

[25] http://wwwmadehowcom/Volume-4/Carbon-Fiberhtml.

[26] http://personalstrathacuk/ashleighfletcher/adsorptionhtm.

[27] Gregg, SJ; Sing, KSW Adsorption, Surface Area and Porosity; 2nd ed; Academic Press: London, 1982.

[28] Kayser, H Wied Ann 1881, 14, 450.

[29] McBain, JW Phil Mag 1909, 18, 916.

[30] Sing, KSW; Everett, DH; Haul, RAW; Moscou, L; Pierotti, RA; Rouquerol, J; Siemieniewska, T Pure Appl Chem 1985, 57, 603.

[31] Dubinin, MM Zh Fiz Khimii 1965, 1305.

[32] Dubinin, MM In Chemistry and Physics of Carbon; Walker, PL Jr, Ed; Marcel Dekker: New York, 1966; Vol 2.

[33] Dubinin, MM In Progress in Surface and Membrane Science; Cadenhead, DA, Ed; Academic Press: New York, 1975; Vol 9.

[34] Lamond, TG; Marsh, H Carbon 1964, 1, 281.

[35] Cheremisinoff, NP; Cheremisinoff, PN Carbon Adsorption for Pollution Control; Prentice Hall: NJ, USA, 1993.

[36] Atkins, PW 5th ed; Oxford University Press: Oxford, 1994.

[37] Cheremisinoff, PN; Ellerbusch, F Eds, Carbon Adsorption Handbook; Ann Arbor, Science Publishers Ins, 1978.

[38] IUPAC J Colloid Interface Chem; Pure Appl Chem 1972, 31, 578.

[39] Characterisation of Porous Solids; Dubinin, MM, Ed; Society of Chemical Industries: London, 1979; Vol 1.

[40] Brunauer, S; Deming, LS; Deming, WS; Teller, E JACS 1940, 62, 1723.

[41] Kiselev, AV J Colloid Interface Sci 1968, 28, 430.

[42] Barton, SS; Evans, MJB; Harrison, BH J Colloid Interface Sci 1974, 49, 462.

[43] Halsey, GD J; Chem Phys 1948, 16, 931.

[44] Kratschmer, W; Rathousky, J; Zukal, A Carbon, 1999, 37, 301.

[45] J W Park, S S Lee, D K Choi, Y W Lee, and Y M Kim, "Adsorption equilibria of toluene, dichloromethane, and trichloroethylene onto activated carbon fiber," Journal of Chemical and Engineering Data, vol 47, pp 980-983, Jul-Aug 2002.

[46] Uyar, T. N., Y; Hacaloglu, J; Besenbacher, F (MAR 25 2009). "Electrospinning of functional poly(methyl methacrylate) nanofibers containing cyclodextrin-menthol inclusion complexes." NANOTECHNOLOGY Vol. 20 (12).

[47] H Fong, I Chun, DH Reneker, “Beaded nanofibers formed during electrospinning”, Journal of Polymer, vol 40, pp 4585-4592, 1999.

[48] A Oya, S Yoshida; Carbon 33, 1995, 1085.

APPENDICES

APPENDIX A

Fiber diameter measurement

A1. Measurement of fibers diameter obtained from SEM

Table A the size of the as-spun fiber is measured in nanometers (nm)

No.	5% PAN	8% PAN	10% PAN	12% PAN	8% PAN 1% Mn	10% PAN 1%Mn
1	141	386	372	750	254	332
2	117	252	328	1369	216	351
3	93	200	431	4462	243	399
4	93	267	347	1529	185	432
5	76	312	431	3643	307	447
6	74	288	474	2399	256	391
7	93	182	451	2957	248	382
8	67	267	464	2128	199	380
9	41	225	363	1319	252	398
10	67	356	408	1746	217	399
11	100	258	453	407	242	423
12	105	258	429	2540	252	399
13	83	221	372	1671	228	387
14	76	221	332	1336	288	378
15	113	288	348	1644	217	434
16	93	435	472	1025	225	402
17	94	288	416	1645	242	384
18	79	283	444	1372	229	435
19	67	182	431	1573	252	423
20	93	288	338	868	185	399
21	93	244	485	2308	269	399
22	93	288	485	4007	227	431
23	83	296	429	2589	273	415
24	148	238	319	727	252	387
25	111	221	431	748	227	391
26	168	225	407	881	225	402
27	117	280	466	2339	210	407
28	159	200	416	1886	257	407
29	100	280	509	3129	229	432
30	79	356	449	3413	253	358
Average	97.2	269.5	416.7	1947.0	238.6	400.2
SD	27.8	57.4	52.2	1020.3	26.9	25.6

Table B the size of the ACNFs is measured in nanometers (nm)

No.	10% PAN 1% Mn carbonized at 800 ℃	10% PAN 1% Mn carbonized at 900 ℃	10% PAN 1% Mn carbonized at 1,000 ℃
1	349	187	252
2	348	222	225
3	370	249	321
4	341	252	247
5	312	225	292
6	444	224	237
7	436	228	257
8	413	172	249
9	393	225	282
10	381	168	207
11	317	251	272
12	363	272	191
13	386	187	218
14	370	213	270
15	399	245	236
16	399	229	206
17	401	193	261
18	431	247	202
19	341	222	210
20	319	236	237
21	370	254	225
22	398	215	196
23	381	227	211
24	282	228	251
25	289	242	286
26	320	213	290
27	354	188	316
28	401	207	257
29	354	223	259
30	399	215	307
Average	368.7	222.0	249.0
SD	41.0	24.7	35.5

Note: For ACNFs formed from 8% PAN 1% Mn could not measure fibers diameter.

APPENDIX B

Toluene breakthrough curve data

B1. Toluene calibration curve obtained from Gas chromatograph

Prepared toluene dissolved in ethylene glycol calculated to concentration ppmv in liquid phase.

Density of toluene is 0.8669 g/cm^3

Density of ethylene glycol is 1.1132 g/cm^3

Table C toluene calibration curve data

Standard Curve							
Conc. (ppm)	Sol. (mL)	Sol (g)	Toluene (g)	Toluene (mL)	Toluene (µL)	g Toluene in 1 µL	Area from GC
0	0.1	0.11132	0	0	0	0	0
2,000	0.1	0.11132	0.00022264	0.000256823	0.256823163	2.2264E-06	2,917,620
5,000	0.1	0.11132	0.0005566	0.000642058	0.642057907	0.000005566	6,346,504
10,000	0.1	0.11132	0.0011132	0.001284116	1.284115815	0.000011132	12,780,432
15,000	0.1	0.11132	0.0016698	0.001926174	1.926173722	0.000016698	19,347,842
20,000	0.1	0.11132	0.0022264	0.002568232	2.56823163	0.000022264	26,018,712

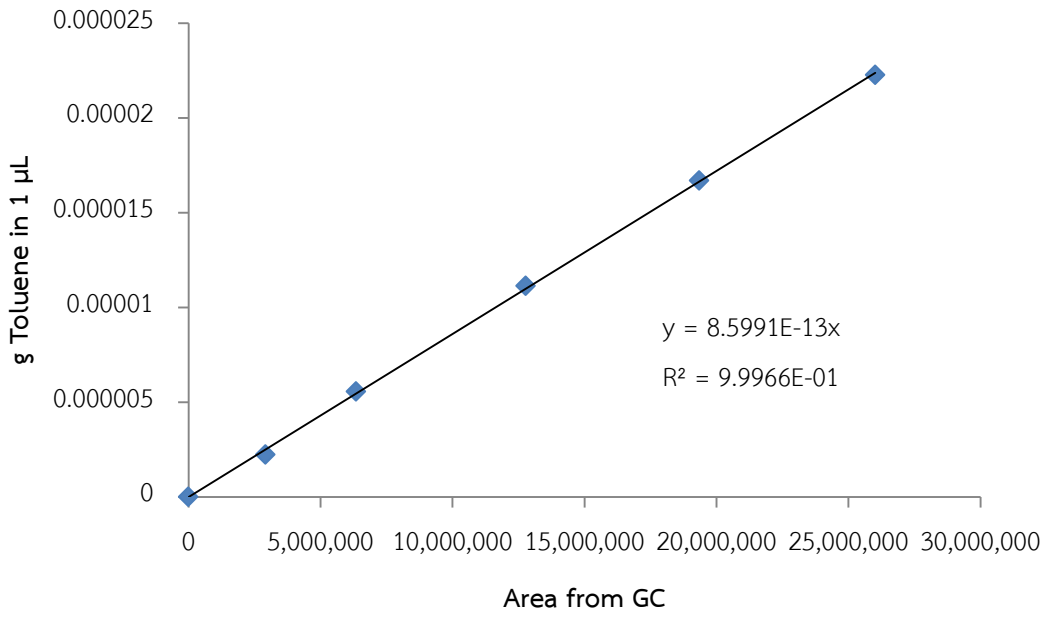

B2. Breakthrough curve of each adsorbent obtained from Gas chromatograph

Table D Breakthrough curve data of ACNFs formed from 8 wt. % PAN 1 wt. %-Mn carbonized at 800 °C.

Sampling Time	Toluene area	Toluene (g)	Toluene (mL)	Toluene (ppmv)	Toluene (mg/L)
Inlet	20,340,872	0.0000175	0.0048	477,570.6790	174.9132
Outlet @10 mins	10,200,469	0.0000088	0.0024	239,490.4656	87.7149
Outlet @20 mins	12,311,701	0.0000106	0.0029	289,058.7683	105.8695
Outlet @30 mins	15,345,408	0.0000132	0.0036	360,285.2876	131.9567
Outlet @40 mins	18,055,644	0.0000155	0.0042	423,917.2325	155.2623
Outlet @50 mins	18,902,548	0.0000163	0.0044	443,801.1646	162.5449
Outlet @60 mins	19,708,782	0.0000169	0.0046	462,730.2311	169.4778
Outlet @70 mins	20,328,397	0.0000175	0.0048	477,277.7862	174.8059

Table E Breakthrough curve data of ACNFs formed from 8 wt. % PAN 1 wt. % Mn carbonized at 900 °C.

Sampling Time	Toluene area	Toluene (g)	Toluene (mL)	Toluene (ppmv)	Toluene (mg/L)
Inlet	20,067,984	0.0000173	0.0047	471,163.7114	172.5666
Outlet @ 10 mins	908,035	0.0000008	0.0002	21,319.1888	7.8083
Outlet @ 20 mins	13,110,121	0.0000113	0.0031	307,804.3747	112.7352
Outlet @ 30 mins	14,252,401	0.0000123	0.0033	334,623.2562	122.5578
Outlet @ 40 mins	15,837,891	0.0000136	0.0037	371,847.9895	136.1916
Outlet @ 50 mins	16,524,568	0.0000142	0.0039	387,970.0516	142.0964
Outlet @ 60 mins	17,526,454	0.0000151	0.0041	411,492.7097	150.7117
Outlet @ 70 mins	19,865,254	0.0000171	0.0047	466,403.9399	170.8233

Table F Breakthrough curve data of ACNFs formed from 8 wt. % PAN 1 wt. % Mn carbonized at 1,000 ℃.

Sampling Time	Toluene area	Toluene (g)	Toluene (mL)	Toluene (ppmv)	Toluene (mg/L)
Inlet	18,669,488	0.0000161	0.0044	438,329.2939	160.5408
Outlet @ 10 mins	464,091	0.0000004	0.0001	10,896.1039	3.9908
Outlet @ 20 mins	638,691	0.0000005	0.0001	14,995.4286	5.4922
Outlet @ 30 mins	8,660,900	0.0000074	0.0020	203,343.8829	74.4759
Outlet @ 40 mins	13,620,971	0.0000117	0.0032	319,798.3041	117.1281
Outlet @ 50 mins	14,136,960	0.0000122	0.0033	331,912.8888	121.5651
Outlet @ 60 mins	14,865,305	0.0000128	0.0035	349,013.2479	127.8282
Outlet @ 70 mins	15,707,585	0.0000135	0.0037	368,788.6160	135.0711
Outlet @ 80 mins	16,705,812	0.0000144	0.0039	392,225.3667	143.6549
Outlet @ 90 mins	16,954,512	0.0000146	0.0040	398,064.4393	145.7935
Outlet @ 100 mins	17,633,177	0.0000152	0.0041	413,998.3926	151.6295
Outlet @ 110 mins	18,433,810	0.0000159	0.0043	432,795.9567	158.5142

Table G Breakthrough curve data of ACNFs formed from 10 wt. % PAN 1 wt. % Mn carbonized at 800 °C.

Sampling Time	Toluene area	Toluene (g)	Toluene (mL)	Toluene (ppmv)	Toluene (mg/L)
Inlet	18,394,776	0.0000158	0.0043	431,879.5017	158.1785
Outlet @ 10 mins	227,094	0.0000002	0.0001	5,331.7987	1.9528
Outlet @ 20 mins	6,615,129	0.0000057	0.0016	155,312.4983	56.8842
Outlet @ 30 mins	10,052,312	0.0000086	0.0024	236,011.9796	86.4408
Outlet @ 40 mins	12,094,852	0.0000104	0.0028	283,967.5055	104.0048
Outlet @ 50 mins	13,570,960	0.0000117	0.0032	318,624.1269	116.6980
Outlet @ 60 mins	13,904,971	0.0000120	0.0033	326,466.1634	119.5702
Outlet @ 70 mins	14,250,740	0.0000123	0.0033	334,584.2586	122.5435
Outlet @ 80 mins	15,126,065	0.0000130	0.0036	355,135.4697	130.0705
Outlet @ 90 mins	15,463,099	0.0000133	0.0036	363,048.4813	132.9687
Outlet @ 100 mins	17,067,944	0.0000147	0.0040	400,727.6387	146.7690
Outlet @ 110 mins	18,269,048	0.0000157	0.0043	428,927.6122	157.0974

Table F Breakthrough curve data of ACNFs formed from 10 wt. % PAN 1 wt. % Mn carbonized at 900 °C.

Sampling Time	Toluene area	Toluene (g)	Toluene (mL)	Toluene (ppmv)	Toluene (mg/L)
Inlet	18,608,592	0.0000160	0.0044	436,899.5546	160.0171
Outlet @ 10 mins	301,621	0.0000003	0.0001	7,081.5718	2.5937
Outlet @ 20 mins	5,051,664	0.0000043	0.0012	118,604.8763	43.4398
Outlet @ 30 mins	8,019,816	0.0000069	0.0019	188,292.2705	68.9632
Outlet @ 40 mins	10,184,911	0.0000088	0.0024	239,125.1890	87.5811
Outlet @ 50 mins	11,129,084	0.0000096	0.0026	261,292.8395	95.7001
Outlet @ 60 mins	12,550,329	0.0000108	0.0029	294,661.3666	107.9215
Outlet @ 70 mins	13,125,571	0.0000113	0.0031	308,167.1157	112.8681
Outlet @ 80 mins	14,035,360	0.0000121	0.0033	329,527.4856	120.6915
Outlet @ 90 mins	15,266,419	0.0000131	0.0036	358,430.7540	131.2775
Outlet @ 100 mins	16,009,347	0.0000138	0.0038	375,873.4983	137.6660
Outlet @ 110 mins	16,237,176	0.0000140	0.0038	381,222.5536	139.6251
Outlet @ 120 mins	18,607,612	0.0000160	0.0044	436,876.5458	160.0087

Table G Breakthrough curve data of ACNFs formed from 10 wt. % PAN 1 wt. % Mn carbonized at 1,000 °C.

Sampling Time	Toluene area	Toluene (g)	Toluene (mL)	Toluene (ppmv)	Toluene (mg/L)
Inlet	17,513,286	0.0000151	0.0041	411,183.5464	150.5985
Outlet @ 10 mins	1,506,236	0.0000013	0.0004	35,363.9780	12.9523
Outlet @ 20 mins	10,425,162	0.0000090	0.0024	244,765.8928	89.6470
Outlet @ 30 mins	12,172,119	0.0000105	0.0029	285,781.6093	104.6693
Outlet @ 40 mins	13,047,963	0.0000112	0.0031	306,345.0057	112.2007
Outlet @ 50 mins	13,548,235	0.0000117	0.0032	318,090.5808	116.5026
Outlet @ 60 mins	15,046,347	0.0000129	0.0035	353,263.8204	129.3850
Outlet @ 70 mins	15,436,214	0.0000133	0.0036	362,417.2651	132.7375
Outlet @ 80 mins	16,408,252	0.0000141	0.0039	385,239.1406	141.0962
Outlet @ 90 mins	15,681,281	0.0000135	0.0037	368,171.0408	134.8449
Outlet @ 100 mins	16,533,584	0.0000142	0.0039	388,181.7327	142.1739
Outlet @ 110 mins	16,910,886	0.0000145	0.0040	397,040.1716	145.4184
Outlet @ 120 mins	17,277,206	0.0000149	0.0041	405,640.7710	148.5684
Outlet @ 130 mins	17,504,728	0.0000151	0.0041	410,982.6185	150.5249

Table H Breakthrough curve data of ACNFs formed from 10 wt. % PAN carbonized at 900 ℃.

Sampling Time	Toluene area	Toluene (g)	Toluene (mL)	Toluene (ppmv)	Toluene (mg/L)
Inlet	17,410,230	0.0000150	0.0041	408,763.9587	149.7123
Outlet @ 10 mins	1,101,454	0.0000009	0.0003	25,860.3532	9.4715
Outlet @ 20 mins	8,604,012	0.0000074	0.0020	202,008.2449	73.9868
Outlet @ 30 mins	14,411,057	0.0000124	0.0034	338,348.2417	123.9221
Outlet @ 40 mins	14,566,392	0.0000125	0.0034	341,995.2556	125.2579
Outlet @ 50 mins	14,999,804	0.0000129	0.0035	352,171.0663	128.9848
Outlet @ 60 mins	15,839,137	0.0000136	0.0037	371,877.2436	136.2023
Outlet @ 70 mins	16,245,344	0.0000140	0.0038	381,414.3250	139.6953
Outlet @ 80 mins	16,325,721	0.0000140	0.0038	383,301.4466	140.3865
Outlet @ 90 mins	16,514,419	0.0000142	0.0039	387,731.7696	142.0091
Outlet @ 100 mins	16,589,760	0.0000143	0.0039	389,500.6540	142.6570
Outlet @ 110 mins	16,599,804	0.0000143	0.0039	389,736.4708	142.7434
Outlet @ 120 mins	16,940,954	0.0000146	0.0040	397,746.1195	145.6770
Outlet @ 130 mins	17,200,858	0.0000148	0.0040	403,848.2438	147.9119

Table I Breakthrough curve data of ACNFs formed from Granule activated carbon

Sampling Time	Toluene area	Toluene (g)	Toluene (mL)	Toluene (ppmv)	Toluene (mg/L)
Inlet	18,568,324	0.0000160	0.0044	435,954.1272	159.6709
Outlet @ 10 mins	9,087,466	0.0000078	0.0021	213,358.9606	78.1440
Outlet @ 20 mins	11,649,466	0.0000100	0.0027	273,510.5647	100.1749
Outlet @ 30 mins	11,910,435	0.0000102	0.0028	279,637.6935	102.4190
Outlet @ 40 mins	12,520,728	0.0000108	0.0029	293,966.3832	107.6670
Outlet @ 50 mins	12,896,291	0.0000111	0.0030	302,783.9932	110.8965
Outlet @ 60 mins	13,995,765	0.0000120	0.0033	328,597.8592	120.3510
Outlet @ 70 mins	14,991,772	0.0000129	0.0035	351,982.4879	128.9157
Outlet @ 80 mins	15,493,368	0.0000133	0.0036	363,759.1484	133.2290
Outlet @ 90 mins	15,937,136	0.0000137	0.0037	374,178.1011	137.0450
Outlet @ 100 mins	17,809,803	0.0000153	0.0042	418,145.2846	153.1483
Outlet @ 110 mins	17,880,414	0.0000154	0.0042	419,803.1163	153.7555
Outlet @ 120 mins	18,206,769	0.0000157	0.0043	427,465.4023	156.5618
Outlet @ 130 mins	18,498,214	0.0000159	0.0043	434,308.0582	159.0680

B3. Toluene adsorption capacity calculation

Toluene (g) = (Toluene (mg/L)) x (Toluene vapor flow rate (mL/min)) x (Adsorption time (min)) x (1 L / 10^3 mL) x (1 g / 10^3 mg)

Toluene adsorption capacity = ∑ ((Inlet Toluene (g) – (Outlet Toluene (g))

VITA

Miss Yanisa Kaewmanee was born in Uttaradit province, Thailand, on July 17, 1984. After completing her high-school study at Uttaraditdaruni School in Uttaradit province, in March 2003. She entered King Mongkut's Institute of Technology Ladkrabang, Bangkok, in June, 2003. After earning the degree of Bachelor of Science in Industrial Chemistry in March, 2007, she got to work in Siam Cement Group in June, 2007. She gained admission to the Graduate School of Chulalongkorn University in June, 2010. She recieved financial support provided by Chulalongkorn University. In July 2014, she was awarded the degree of Master of Engineering in Chemical Engineering.